Applied Energy 282 (2021) 116041

Contents lists available at ScienceDirect

Applied Energy

journal homepage: www.elsevier.com/locate/apenergy

Additive manufacturing for energy: A review

Cheng Sun [a], Yun Wang [b], Michael D. McMurtrey [a], Nathan D. Jerred [a], Frank Liou [c], Ju Li [d]

[a] Idaho National Laboratory, Idaho Falls, ID 83415, USA
[b] Department of Mechanical and Aerospace Engineering, The University of California, Irvine, CA 92697, USA
[c] Department of Mechanical and Aerospace Engineering, Missouri University of Science and Technology, Rolla, MO 65409, USA
[d] Department of Nuclear Science and Engineering and Department of Materials Science and Engineering, Massachusetts Institute of Technology, Cambridge, MA 02139, USA

HIGHLIGHTS

- AM technologies have great potential to address global energy challenges.
- AM technologies are applied in nuclear energy, battery, fuel cell, and oil & gas.
- The challenges of deploying AM technologies in the energy sectors are reviewed.
- Fundamental research needs and future directions are outlined.

ARTICLE INFO

Keywords:
Additive manufacturing
Nuclear energy
Battery
Fuel cell
Oil & gas

ABSTRACT

The conflict between rapidly growing global energy demand and climate change is a grand challenge that requires significant science and technology innovations. Advanced manufacturing could extensively drive down greenhouse gas emission and pollution, and shorten the time-to-market. Additive manufacturing is a process of fabricating three-dimensional objects by depositing materials layer-by-layer directly from computational geometry model, and it eliminates the design and fabrication restrictions of conventional manufacturing methods to a large extent. As an emerging and transformative technology, additive manufacturing technologies have shown the potential benefits of energy saving in multiple energy sectors. To further increase their applications in nuclear energy and renewable energies, fundamental research is needed to overcome some key challenges in terms of process monitoring and control, dimension accuracy, and structural integrity of the components. The validation and qualification of additive manufacturing processes and the products from those additive manufacturing processes are imperative to meeting the high standards of critical components in various energy production, conversion and storage systems. In this review article, we summarize the current status of cutting-edge additive manufacturing technologies and their applications in the fields of nuclear energy, battery, fuel cell, oil & gas. We also outline the major challenges and fundamental research needed to achieve the full potential of additive manufacturing technologies. This review provides critical discussion and prospects to address global energy challenges by applying innovative additive manufacturing technologies.

1. Introduction

The global energy demand is expected to grow by nearly 50% between 2018 and 2050, and the industrial sectors, including manufacturing, refining, mining, agriculture, and construction, project more than 30% increase in energy usage [1]. This rise is demanded by the rising living standards, especially of the great majority of people living in non-first-world countries, but it runs into sharp conflict with the requirement that the global CO_2 emission must be halved by 2030–2040, according to the 2018 Intergovernmental Panel on Climate Change (IPCC) report "Global Warming of 1.5 °C". How to manage this seemingly impossible balance is the topic of the "MIT A + B Applied Energy Symposia" conference series that aim to highlight technical and socioeconomic solutions, with "A-Action before 2040" and "B-Beyond 2040 technologies", without which there will be dire, irreversible environmental and socio-economic consequences in the coming

E-mail addresses: cheng.sun@inl.gov (C. Sun), yunw@uci.edu (Y. Wang), michael.mcmurtrey@inl.gov (M.D. McMurtrey), nathan.jerred@inl.gov (N.D. Jerred), liou@mst.edu (F. Liou), liju@mit.edu (J. Li).

https://doi.org/10.1016/j.apenergy.2020.116041
Received 15 May 2020; Received in revised form 8 September 2020; Accepted 7 October 2020

decades. Advanced manufacturing, especially aiming at clean and scalable energy technologies such as nuclear [2], solar [3], wind [4] and energy storage [5], will be a key part of the solution. Traditional manufacturing processes are labor and capital intensive, and rigid and mono-purpose. Advanced manufacturing is (a) labor saving, (b) flexible, and (c) fast to deploy, also potentially scalable, which has to be the case if it is to have any real impact on the climate-change challenge outlined above, because we must turn the ship of the global economy and ~20TW energy industry within 10–20 years.

Additive manufacturing (AM) is a process of fabricating objects layer-by-layer from computer-generated three-dimensional (3D) geometry models, without the constraints of conventional casting, forging, and machining processes. AM technologies have shown a great potential to reduce the energy consumption embedded in manufacturing by reducing materials wastage and eliminating machining steps. It has been reported in the literature that the widespread implementation of AM technologies would lead to a significant reduction of the global energy demand by as much as 27% [6]. In recent years, AM technologies have been increasingly applied in various energy sectors to improve the material performance and enhance energy efficiency and have been considered as one of the next-generation solutions for energy generation, conversion and storage. In nuclear power plants, AM enables the field fabrication of parts and expedites the deployment of nuclear core components for the current reactor fleets and future advanced reactors. Westinghouse has implemented powder-bed fusion AM technologies in nuclear power plant components manufacturing and printed 316L stainless steel, Inconel 718, and Zr alloys as nuclear reactor components [7]. AM techniques can also be used to fabricate functional composites to tailor the electrochemical properties of fuel cells. Hughes et al. reported a technique to incorporate $MoSe_2$/C and Pt/C into polylactic acid to obtain filaments using materials extrusion-based AM process, and their electrochemical properties towards hydrogen evolution reactions and oxygen evolution reactions are greatly improved [8]. A consulting firm, GlobalData, predicts that AM in the oil & gas sector is expected to reach over $60 billion worldwide by 2030 [9]. The use of a direct metal laser melting technique has allowed GE oil and gas to manufacture NovaLT 16 gas turbines with different design concepts and reduce the development and validation time by over 50% [10]. Electron-beam melting (EBM) has been shown to be capable of repairing surface damages of single-crystalline turbine blades made of Ni-based superalloy, with no change in the γ/γ' microstructure in the melt-pool region, opening avenues to printing large single crystals with creep and helium resistant [11]. Fig. 1 shows some examples using AM in the fields of nuclear energy, battery, fuel cell, oil and gas.

In this paper, the current progress in AM technologies, with a focus on direct energy deposition, powder-bed fusion, materials extrusion, and vat photopolymerization, are first reviewed. Then, the applications of AM technologies in the fields of nuclear energy, batteries, fuel cells, oil and gas are summarized. Although AM technologies have also been applied in many other energy sectors, such as wind, solar, and hydroelectric energy [12], we focus on the major energy consumption sources (oil & gas and nuclear energy) and primary energy storage devices (batteries and fuel cells) in this review paper. Afterwards, the major challenges of deploying AM technologies in these application fields are evaluated, including in-situ process monitoring, fabrication of feedstock, surface roughness, structural integrity, cost, and durability. We also highlight the fundamental needs to validate and qualify AM processes for robust energy systems. Finally, we envision the future research directions in different energy sectors.

2. Additive manufacturing technologies

AM techniques are capable of fabricating a wide variety of materials, including ceramic, glass, metals, polymers, and composite materials. Laser- and electron-beam-based power sources are two popular power sources used in AM processes. Various AM techniques, such as direct energy deposition (DED) [19], powder-bed fusion (PBF) [20], materials extrusion [21] etc., have been successfully applied to fabricate materials and components for energy systems. In addition, friction stir welding-based techniques such as friction stir additive manufacturing (FSAM), where mechanical energy is used for consolidation, provides high build rate, less porosity and can build large parts, and are under active development. The major AM techniques that show promising applications in the energy of nuclear, batteries, fuel cells and oil & gas are summarized here and listed in Table 1.

2.1. Directed energy deposition (DED)

DED is an AM process where focused thermal energy (laser, electron beam, plasma-arc and electric-arc) is used to fuse powders or wires by melting as they are deposited on the substrate [19]. The DED process allows for the production and repair of parts and has been used

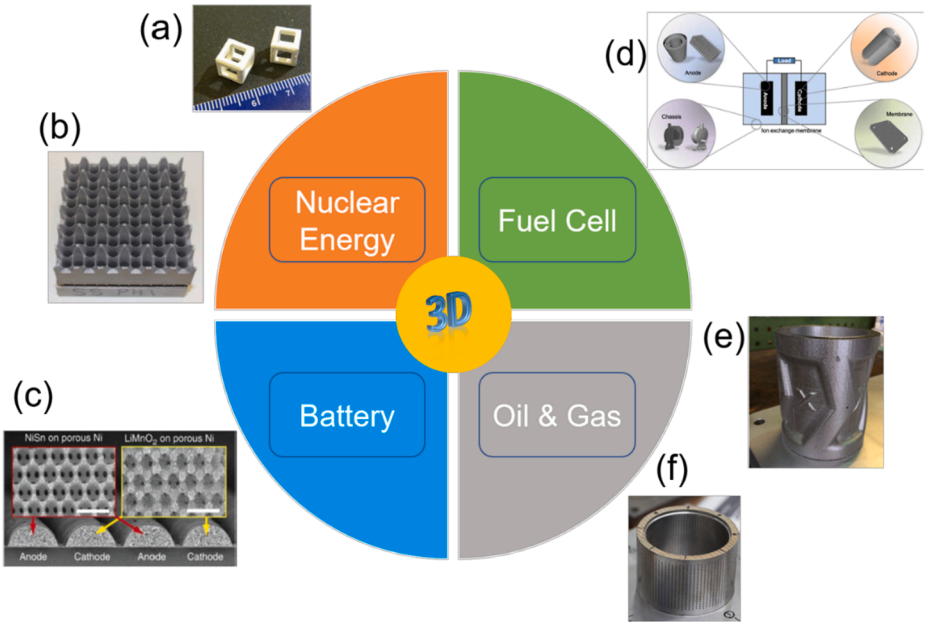

Fig. 1. AM-fabricated materials, components, and products in four major energy sectors. (a) Thorium dioxide nuclear fuel fabricated with a stereolithography-based AM technique [13]. (b) Nuclear fuel assembly debris-filtering bottom nozzle 3D printed by Westinghouse [14]. (c) Interdigitated electrodes of a micro-battery fabricated using template-assisted electrodeposition [15]. (d) Membrane and anode components of a microbial fuel cell were fabricated with fused deposition modeling [16]. (e) A nozzle component used metal AM to include down-hole cleanouts of oil and gas wellbores made by EnergyX [17]. (f) Masoneilan control valve parts with special configurations were fabricated with metal laser sintering by GE Oil and Gas [18].

Table 1
Examples of AM applications in the selected energy sectors.

AM Techniques	Materials/Components	Improved/Unique Properties	Energy Application	Reference
DED	Inconel 718	Mechanical properties and energy storage capacity	Nuclear energy, Oil & gas	[44]
	316L stainless steel	Enhanced resistance to IASCC	Nuclear energy	[22]
	High-entropy alloy AlCoCrFeNi	Resistance to void swelling	Nuclear energy	[26]
	Oxide dispersion strengthened 14Cr stainless steel	Resistance to creep	Nuclear energy	[45]
PBF	316L stainless steel	Better radiation tolerance and lower IASCC susceptibility.	Nuclear energy, Oil & gas	[46,47]
	17-4 PH stainless steel	Higher corrosion resistance	Oil & gas	[48]
	Aluminum 6061	Crack-free	Nuclear energy, Oil & gas	[49]
	Graphite-Carbon fiber bipolar plate	Improved strength with satisfied electrical conductivity	PEM fuel cell	[50]
	AlSi10Mg	Cellular anodic structure	Microbial fuel cell	[29]
	Graphite composite bipolar plates	Satisfied application requirements of PEM fuel cells	PEM fuel cell	[51]
Materials Extrusion	Holey graphene oxide	Enhanced Li–O2 battery performance	Li-ion batteries	[31]
	(Graphite/PLA)/Li	Enhanced the electrochemical performances with sufficient strength	Li-ion batteries	[32]
	Lithium iron phosphate (LFP), lithium titanium oxide (LTO)	High capacity and good cyclability	Li-ion batteries	[33]
	Lithium Nickel Manganese Cobalt Oxide Cathode	Enhanced Li-ion Transport in Thick Battery Electrodes	Li-ion batteries	[34]
	Sulfur copolymer-graphene architectures	High reversible capacity and good cycle performance	Li-S batteries	[35]
	Yttria-stabilized Zirconia electrolyte	Crack-free electrolyte planes	Solid oxide fuel cell & electrolyzer	[52]
	Gel-lay and polymer anode	Stable level of power output	Microbial fuel cells	[16]
Vat Photopolymerization	Microfluidic to millifluidic devices	Acceptable transmittance with continuous nitrate analysis	Microfluidic fuel cell	[53]
	Microfluidics device	Commercialization	Microfluidic fuel cell	[37]
	Yttria-stabilized Zirconia electrolyte	Comparable power density	Solid oxide fuel cell	[38]
	Lithium titanate / Lithium iron phosphate	High reversible specific capacity and high pulse-power capability.	Micro-battery	[54]

throughout the entire product lifecycle for applications ranging from materials research to functional prototyping to volume manufacturing. Discovery and design of advanced materials with excellent irradiation tolerance and corrosion resistance are crucial for developing the next generation nuclear energy systems. DED techniques have been used to print structural materials and coatings for nuclear applications. 316L stainless steels have been printed with DED processes, and the printed 316L specimens show an enhanced resistance to irradiation-assisted-stress-corrosion-cracking (IASCC) [22]. High-entropy alloys (HEA) are gaining interest in nuclear energy systems due to the improved irradiation tolerance and corrosion resistance [23–26]. $Al_xCoCrFeNi$ HEA coating were successfully deposited on a high-temperature stainless steel substrate using a DED process. The microstructure and mechanical properties of the HEA coating can be tuned by the printing parameters [25]. The advantages of DED processes include the ability to fabricate dense metal parts with good metallurgical properties at reasonable production speeds and the capability for weld and repair structural components, while rough finishing surface, high equipment cost, and residual stress are the major issues.

2.2. Powder-bed fusion (PBF)

PBF is an AM process where a heat source (a laser or electron beam) selectively fuses or melts layers of powdered materials to form solid 3D objects [27]. Selective laser sintering (SLS), a class of PBF, was first done on polymers and nylon. The powder needs fine grains with thermoplastic properties, so that it becomes viscous, flows, and solidifies quickly. Afterwards, a variety of materials were fabricated using PBF processes, such as direct metal laser sintering (DMLS), selective laser melting (SLM) and EBM [28]. Microbial fuel cell (MFC) is a device that generates energy by bacterial processes from renewable stocks/waste. To improve the power efficiency, SLM process was used to fabricate the critical components in MFCs, including a bio-inspired lattice aluminum alloy anode and a 3D macro-porous structure with high specific surface area and a surface roughness ideal to host the microbes. An optimal energy recovery close to 3 kWh /m^3 per day was achieved [29]. The PBF process is capable of fabricating functional parts in essentially final components with complex geometry for energy systems. The disadvantages of this AM process include the relatively high cost of the machines and operation, slow production rate, and the shrinkage of fabricated parts.

2.3. Materials extrusion

Material extrusion produces 3D structures by extruding filaments through a heated nozzle, melting and depositing materials layer by layer on substrates. The fused deposition modeling (FDM) process [30], a representative material extrusion process, is a non-laser filament extrusion process that utilizes engineering thermoplastics, which are heated from filament and extruded in layers to build the model. The models can be made from Acrylonitrile butadiene styrene (ABS), Polycarbonate, Polyphenylsulfone (PPSF), and various versions of these materials. The FDM has been widely used to fabricate components for energy storage devices [31–35]. In lithium ion batteries, an FDM printed graphite/polylactice acid (PLA) filament was used to mitigate the interdiffusion issues of electrodes. A graphite/PLA filament was printed using FDM and used as negative electrode in a lithium-ion battery. Graphite content, used as active material into the filament, was increased as high as possible to enhance the electrochemical performances without sacrifices of mechanical strength. A reversible capacity was achieved with values reaching 200 mAh/g of active material at current density of 18.6 mA/g after 6 cycles [32]. The material extrusion-based processes enable efficient materials management, not wasting much material during and after printing. The cost of the extrusion molding and materials used in these processes are relatively low, and more material options are available compared to other AM techniques. The unpredictable shrinkage of products limits its application for large-size components.

2.4. Vat photopolymerization

Vat photopolymerization works by the principle of solidifying a vat

of photopolymer resin through polymerization, layer-by-layer to develop a 3D object [36]. Stereolithography (SLA) and digital light process (DLP) are the two most common forms of vat photopolymerization. SLA uses ultraviolet (UV) laser light to cure photopolymer resin, while DLP uses a projector as the light source. The typical photocurable resin includes epoxy, vinylether and acrylate. Acrylics only cure to about 75 or 80%, since curing stops as soon as the light source is removed, while epoxies continue to cure even after the light source is switched off. Vat photopolymerization has been demonstrated in the fabrication of components in poly(dimethylsiloxane) (PDMS) microfluidic fuel cell devices, for example, SLA was used as an automated fabrication technique that allows for producing complex 3D geometry in a single polymeric materials at medium-volume throughputs [37]. Solid oxide fuel cell (SOFC) is a high-temperature fuel cell with solid ceramic electrolyte sandwiched by electrodes and can be operated using a wide range of fuel sources. An 8 mol.% yttria-stabilized-zirconia (8YSZ) electrolyte for SOFC was successfully fabricated by DLP-stereolithography method, and the electrochemical performance is comparable to that to the same cell with 8YSZ electrolyte fabricated by conventional dry pressing method [38]. In general, vat photopolymerization processes show the advantage of smoothness of liquid surface in steady state and can be used to fabricate parts with high precision of surface quality. The major disadvantage is the limitation of materials that needs to be photo curable.

2.5. Other AM technologies

Some other AM technologies have also been used to fabricate core components in the energy systems. Material jetting is an inkjet printing process whereby a printhead dispenses droplets of a photoreactive material that deposits onto a build platform layer upon layer and solidifies under UV laser light [39]. This process has been largely adopted to print batteries. In lithium-ion batteries, silicon nanoparticle anodes with poly (3,4-ethylenedioxythiophene)-poly(styrene sulfonate) polymer binders were fabricated by inkjet-printing, and these anodes exhibit high capacities larger than 1700 mAh/g for 100 cycles and stable cycling performance at depth-of-discharge of 1000 mAh/g over 1000 successful cycles [40]. $LiCoO_2$ thin film electrodes with thickness of ~1.2 μm were prepared by inkjet printing process, and the electrochemical testing shows that at discharge current density of 180 $\mu A/cm^2$, the discharge capacity was only lost 5% after 100 charge–discharge cycles [41]. Material jetting can achieve multi-functional products with high precision of geometry and good surface finishes, while the materials option for this process is limited. Binder jet printing is an AM technique that dispenses liquid binding agent on powdered materials to build a 3D physical article with high production rate [42]. Binder jetting shows great potentials to be widely used in fuel cell application. Manogharan et al. reported the feasibility of using binder jetting process to fabricate a complete SOFC unit with a Ni-YSZ anode, LSM-20 cathode and 8YSZ oxygen ion-conducting electrolyte [43]. The limitation of this process is the significant part shrinkage, low geometry accuracy and density of parts. Post-printing treatment is required to maintain the mechanical properties.

3. Applications of additive manufacturing in energy sectors

3.1. Nuclear energy

Nuclear energy is looking to AM, along with other advanced manufacturing techniques, to provide design flexibility, reduce costs, and shorten timelines for the production of components that make up a nuclear power plant [55,56]. While other methods for nuclear energy components, such as powder metallurgy (specifically hot isostatic pressing), are more developed, AM is a fairly new area of interest for nuclear energy [55]. AM has the benefit of allowing for constant process monitoring of each layer of material as it is manufactured, allowing for improved manufacturing control and the collection of detailed information about the properties of the final component [57]. Another benefit of AM is the ability to transition materials more seamlessly (gradual transitions and narrow fusion zones with minimized heat-affected zones) than traditional joining (brazing, welding, or soldering) or to create functionally graded compositions [57,58], or even fully 3D patterned phase-, grain size-, and composition-distributions aimed at optimizing the microstructure-properties relationship. Material transitions are particularly common in nuclear plants, as there are large variations of pressures, temperatures, and radiation doses, resulting in the need to employ a variety of materials. AM has been demonstrated to create graded compositions of many types of materials, such as Inconel to steel, copper to steel, titanium alloys to steel, as well as titanium alloys to carbide materials [58–63]. Modeling and simulation efforts have helped progress this work and increase the feasibility of functionally graded compositions [61,64–66], and even 3D printed micro-composites.

The United States Department of Energy Office of Nuclear Energy (US DOE-NE) funds work in this area through the Advanced Methods for Manufacturing (AMM) under the Nuclear Energy Enabling Technologies (NEET) program [67]. The goal of the AMM program is to conduct research that leads to innovations in manufacturing that reduce costs and time needed for constructing new nuclear power plants, as well as increases the reliability of components. Various companies and labs are working under DOE awards to make AM feasible for the nuclear industry, such as Novatech and BWXT [68]. The Nuclear Regulatory Commission held a public meeting on AM for reactor materials and components in 2017 and invited over 20 companies, labs, standards organizations, and governmental bodies [69]. Industry attendees who expressed interest in pursuing AM for nuclear applications included NEI, EPRI, GE, Westinghouse, Novatech, NuScale, and Rolls Royce and range from interest in light-water reactors to more advanced reactors, such as the small, modular reactors. AM can be used for rapid prototyping, a cost-saving method of examining components prior to full-scale production, as well as the actual component production. In nuclear energy, there are several areas of interest where AM components may be used.

Structural components within a nuclear reactor must typically meet requirements set by specific codes and standards, such as the American Society of Mechanical Engineer (ASME) Boiler and Pressure Vessel (BPV) codes for pressure-retaining components. As many codes and standards do not currently allow AM components, much of the work for using AM in structural components remains at the lab level. This should change in the future, as there are committees such as the American Society of Testing and Materials (ASTM) F42 technical committee and the ASME Special Committee on the use of Additive Manufacturing for Pressure Retaining Equipment that are seeking to set the rules for use of AM within their respective codes and standards. There are several areas of interest in the use of AM in structural components. The microreactor is focused on space-saving methods to decrease the overall reactor size and has turned to AM as a method to create complex and compact parts, such as compact heat exchangers. Work has also been performed to examine AM for use in creating complex components for the International ThermoNuclear Experimental Reactor (ITER) for nuclear fusion reactor program [28].

Most reactor internals are not pressure-retaining components and do not fall within the restrictions of the ASME BPV code, therefore, AM work has progressed more significantly in the area of actual application in nuclear power plants. There is interest in AM for reactor core internals, including manufacturing of fuel, cladding, control elements, etc. Westinghouse was one of the first to consider installing actual AM components into a reactor, choosing to install a thimble plugging device made of AM 316L steel. Significant work is being performed within research and test reactors to better understand the performance of AM components. Oak Ridge National Laboratory has explored the use of AM to manufacture control elements for the High-Flux Isotope Reactor (HFIR) [70,71] and Idaho National Laboratory has used AM capsules for

tests inside the Advanced Test Reactor. Similar to the structural components, the benefits from AM include the ability to create complex designs, rapidly prototype, and transition between dissimilar materials. For some exotic materials, such as those used in nuclear fuels, there are additional benefits, such as using the AM energy source not only for manufacturing the structure of the fuel but also for reducing or modifying the fuel composition, such as in the conversion of UF_4 to U_3Si_2, an accident tolerant fuel [72]. In this case, there are additional benefits, such as using less equipment for fuel fabrication from cradle to fuel product, as well as less raw material input and minimizing the facility footprint. It also has the potential to improve the economics, as traditional manufacturing routes would include an additional step of converting the UF_4 to uranium metal prior to the formation of U_3Si_2. AM has found applications in other areas related to nuclear energy outside of the plant itself. One such application is the use of AM in the reprocessing of spent fuel. Spent nuclear fuel is a significant challenge for the nuclear energy industry. One method for overcoming this problem is to recycle the spent fuel and use it again in reactors. AM has been demonstrated to manufacture complex, fluid devices with internal channels, as well as a full array of 1.25-cm diameter rotor centrifugal contactors for small-scale demonstrations of separation techniques aiming to remove minor actinides from used nuclear fuel [73]. In this case, AM was used to simplify the fabrication processes and reduce the level of needed materials and human effort.

3.2. Batteries

Lithium-ion batteries (LIB) consist of many repeats of 5 basic layers: anode current collector (copper), anode (anode-active material, binder, conductive agent + solvent↑), electrolyte/separator, cathode (cathode-active material, binder, conductive agent + solvent↑), cathode current collector (aluminum). In this sense, traditional LIBs are already fabricated by a roll-to-roll "printing" process and then layer-by-layer stacking or winding. When the anode/cathode slurry was transferred to the current collector, they were in the form of inky fluid; but after the solvent evaporated, the slurry turned in a solid layer ("ink drying"). Because this solid layer paste is so thin (a single period of these 5 layers is usually 150 μm or so, and can be as thin as $d = 70$ μm), and the maximum tensile strain sustained when bending over a radius-R roller is $d/2R$, the layers can be bent and wound without fracturing the solid "dried ink" for large enough R. This can be taken as an advantage of thin and flexible printed batteries. While traditional batteries have well-defined cylindrical or orthorhombic shape factors, with printable batteries it is possible to achieve arbitrary 3D shape (that for instance, can fit into the irregularly shaped vehicle chassis). In addition, it is possible to integrate printed battery with printed electronics, and both can be mechanically flexible.

Custom printed batteries share many common characteristics with printed electronics, such as relatively lower-performance compared with conventional high-production-volume parts, with relatively eco-friendly disposal and are usually required to be flexible/wearable with high degree of customizability. Printed batteries can be thin and used in small devices. Printed batteries have diverse applications today, such as in disposal packaging like coffee cups, clothing, backpacks, etc. giving day-to-day objects the ability to communicate in Internet of Things (IoT). Co-design of printed electronics and printed battery in one package gives higher performance and reduce cost, as for example the extra edge-seal would be eliminated. Inks are transferred via inkjet printhead, screen printing, stencil printing [74], extrusion printing [75], flexographic printing [76] etc. The initial fluidity of the ink is necessary for the printing pattern versatility. For the transfer of fluid to solid to happen in expected manner, viscosity, surface energy and wetting properties of the ink are also key besides the lithium ion-storage/transport aspects. The ink then needs to be dried, and the process repeats once or twice so the electrolyte layer and/or cathode layer goes on top. Finally, the battery must be sealed. The printed battery can be use-once ("primary battery") or rechargeable ("secondary battery") in applications.

It is possible to get rid of the copper and aluminum foil in the current collectors, and produce so-called "free-standing" [77] electrodes by printing [78], with embedded current collector in the form of 3D percolating network of carbon nanofibers (CNF) or nanotubes (CNT). This reduces the 5 basic layers of a period to 3 basic layers, by merging the current collector layer with the adjacent active-electrode layer. The elimination of metal foils means 3D all-printed batteries are possible, as the electrolyte layer can also be made from castable or printable inks [79], thus no mechanical lay-down of foil is necessary (in principle, it is also possible to 3D-print metals by electron or laser melting of 10 μm scale powders, but these are high-temperature processes that require further development). This absence of metal foils comes with a price, however. The ~10 μm copper foil and aluminum foil (coated double sided, thus counting only ~5 μm per single period) play both an electrical and a mechanical function. Their room-temperature electrical conductivity per weight is still at least an order of magnitude better than the best CNT rope, and there is also a percolation problem associated with the filler volume fraction [80]. Consequently, the electrical conductivity of the printed free-standing electrode is only about 10 S/cm even with about 40% CNFs. With copper (6×10^5 S/cm), even considering the volume dilution effect (5 μm → 100 μm), the effective electrical conductivity is still 30,000 times better than the 10 S/cm. Granted, the electronical conductivity of 10 S/cm is still much better than the ionic conductivity of 0.37 mS/cm [81], so vertical transport of electron is not a problem. But lateral transport of electron could become problematic. Consider internal resistance arising out of Li^+ transport across a 20 μm gel electrolyte and lateral length scale L: $L \times 0.37$ mS/cm / 20 μm = $L \times 1850$ S/m^2. If this becomes comparable to electron transport across this lateral length L: 100 μm × 10 S/cm / L, we will have a problem with long-range lateral electron transport. Solving the above gives $L_c = 7$ mm. Thus, if the lateral footprint is longer than a centimeter or so, electronic contribution to cell's internal resistance could become more than the ionic contribution (which we know is a huge problem already), for the metal-free 3-layer design, whereas it was not a problem at all for the 5-layer with-metal design. This scaling is highly relevant for small cell design – it means even with 3D electrodes, metallic structures must be erected as an interconnected grid at least every centimeter or so for long-range lateral electron percolation, whereas everything within 1 cm or so can be 3D printed without metal.

For mechanical flexibility, Kohlmeyer et al. used a lot of binder component in the active materials layer to give the free-standing layer mechanical strength. Brittle behavior was found in conventional dried cathode ink with typically 90% cathode-active content and only 5% binder [78]. With more binder content (up to 40–50%) in the dried ink, a tensile strength can reach a few MPa or even better. It is seen from the Fig. 2 that the Young's modulus of the $Li_4Ti_5O_{12}$/CNF/PVDF dried ink is of the order 1 GPa (neat PVDF binder has modulus 2.5 GPa). There appears to be significant inelastic component, and reversible tensile strain range of perhaps about 1%. This then means the radius of curvature in bending should not be less than about 50 × the thickness for this to be purely elastic. This comes to $R_c = 1$ cm or so (say the thickness $d = 200$ μm). Note, however, that R_c here is defined more like a "fatigue threshold", that is, no damage is generated at all if bent up to this curvature. It is possible that local inelasticity or fractures occur ("mud cracks", etc.) and so there are local damage accumulation when bent to more than $1/R_c$, but these damages accumulate gradually and are not immediately catastrophic.

Such damage accumulation behavior (not catastrophic failure) with repeated gentle bending and creasing [82] (extreme bending) has been studied. Multi-walled CNT (MWCNT) is used as the substrate, which is potentially printable instead of using aluminum or copper foils. Indeed, with $R = 0.788$ cm bending, very little damage accumulation is seen, but with $R = 0.4$ cm bending, voltage drop starts to happen with tens of cycles. The batteries are also creased (effective radius of curvature may

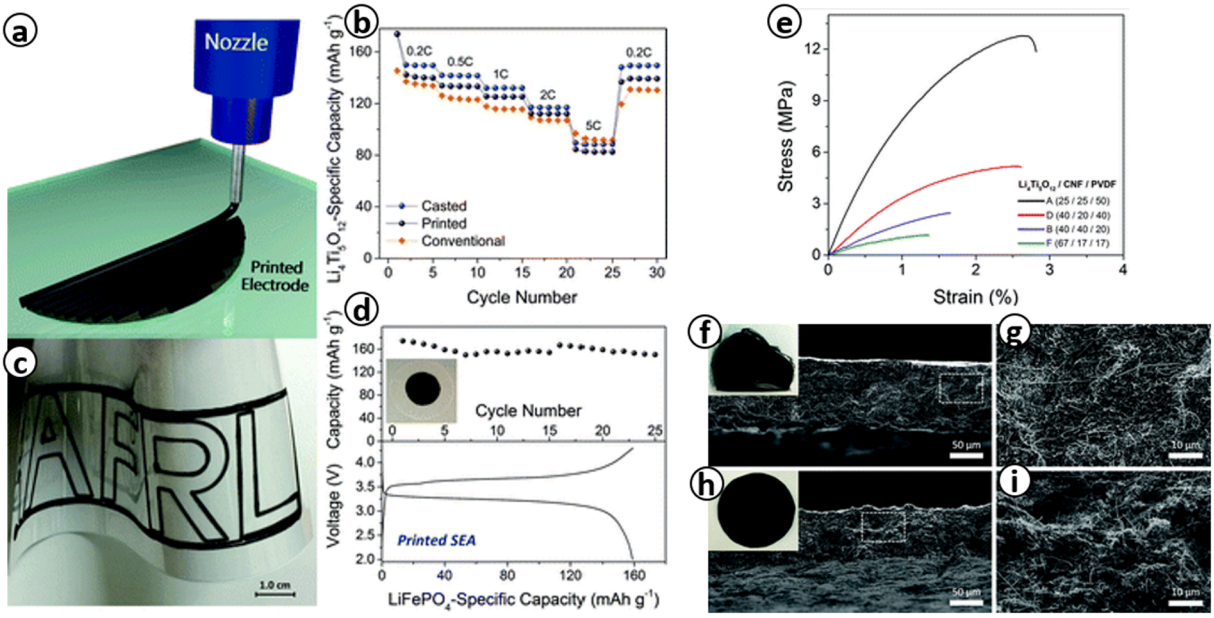

Fig. 2. Direct ink writing printing of lithium ion battery electrode. (a) Printing of active/CNF/PVDF composite electrodes at a mass ratio of 40:40:20. (b) Rate performance of printed, casted composite and a conventional $Li_4Ti_5O_{12}$ electrode on copper under active loading between 3.0 and 3.5 mg/cm^2. (c) Photograph of a complex filamentary printed design. (d) Cycle performance and charge/discharge profile with a photograph (inset) of a fully printed separator electrode assembly. (e) Representative uniaxial tensile stress–strain curves of $Li_4Ti_5O_{12}$/CNF/PVDF composites with four different mass ratios. (f-g) Photograph and cross-sectional scanning electron microscopy (SEM) images of the composite with mass ratio of 25:25:50. (h-i) Photograph and cross-sectional SEM images of the composite with mass ratio of 40:40:20 [78].

be mm) at progressively different locations, and the MWCNT system can sustain 288 creasing with overall electrochemical function intact. In contrast, with the same creasing protocol, the metal current collector electrodes have shown significant powder spallation in the case of copper foil (due to adhesion problems between electrode and copper foil), whereas the aluminum foil has sustained fatigue fracture itself (but without much powder spallation). Mechanically, the 3D CNF/CNT electrodes could have better fatigue tolerance because the powder materials interpenetrate into the 3D network (thus better adhesion than with metal foils which only contact at the surface); the 3D network itself is also polymeric and can sustain creasing better than metals.

Lastly, we discuss about the processing options. Cobb and Ho mentioned that "Inkjet printing, while a popular concept, is perhaps the least well-suited technology for mass producing printed batteries."[75]. This is because the print head is quite a distance away from the substrate, and the ink liquid needs to fly as a free-standing fluid droplet before it hits the substrate (the definition of inkjet), and for such solid-rich ink (if the solvent is too much, the drying time will be longer) free droplets outside a certain size range are difficult to handle (easy to clog the inkjet head, or making a splatter). A simple calculation explains why: 1200 dpi (drops per inch) means 2.54 cm/1200 = 21 μm. State-of-the-art inkjet nozzle (actuated by piezoelectric) are designed to eject 3D droplet on the order of 10 μm. But in some sense, 10 μm is a bit too small for printed battery. Cathode secondary particles (solid) are often few microns in size. Generally, the nozzle diameter needs to 10 particle diameters or more to avoid clogging or jamming, thus these standard inkjet heads are easily clogged. One may take larger nozzles, but then the fluid shape / splatter / speed becomes more difficult to control. Cobb and Ho recommended spray printing (that also uses droplets) instead of inkjet printing.

In above, only a single homogenous ink material was used. In order to coat multiple layers, there must be multiple passes, and registration or alignment of layers is an issue. Co-extrusion method was developed by Palo Alto Research Center (PARC) to lay down multi-materials ink in one pass, like "gel striped toothpaste" [75]. It uses a dispenser needle or needles. The difference between dispenser and inkjet nozzle is that the disperser is almost touching the substrate like a brush/dip-pen and the printing occurs continuously ("vectoring") instead of in droplet format ("rastering"). 3D structured electrodes can also be printed this way, as shown in Fig. 3.

3.3. Fuel cells and electrolyzers

Fuel cells are energy converters that convert the chemical energy stored in a fuel to electricity directly through electrochemical reaction. AM technologies have been employed to fabricate components for fuel cells, including biological fuel cells (BFC), polymer electrolyte membrane (PEM) fuel cells, reversible fuel cells, and microfuel cells. BFCs, utilizing microbes or enzymes for energy conversion through biological metabolisms, are promising in applications to water quality monitoring, and data processing/transmission in remote or harsh environments. Microbial fuel cells (MFC) and enzymatic fuel cells (EFC) are typical BFCs, which have been fabricated using AM, for chambers, membranes [84], and high-performance electrodes with a large reaction area, high conductivity, biocompatibility, and multiscale, porous structure [85,86]. Calignano et al. [29] developed a fully AM-based MFC with open pores for hosting microbes (Fig. 4) and achieved an optimal power of about 3 kWh m^{-3} per day. Bian et al. [87] employed 3D printed porous copper electrodes as MFC anode, which performed about 10-fold higher efficiency than copper-mesh anodes. Zawadzki et al. [88] printed an MFC with an exchangeable membrane to demonstrate the potentials of AM in MFC applications. AM techniques simplify the MFC design and assembly by eliminating clamps, screws, clips, gaskets, or sealants. AM is suitable for fabricating biocompatible components, and thus has been considered for implantable or wearable BFCs applications [89–91]. PEM fuel cells are promising for automobiles, portables, and small stationary applications with a practical efficiency as high as 65% and water as the only byproduct [92]. AM is capable of fabricating the bipolar plate (BP) and the balance of plant (BOP) components [93–95]. BPs provide multiple functions including mechanism support, electric current collection, heat removal, and gas distribution and water removal via the embedded gas flow channels (GFC). A single BP is usually about 1–2 mm thick with

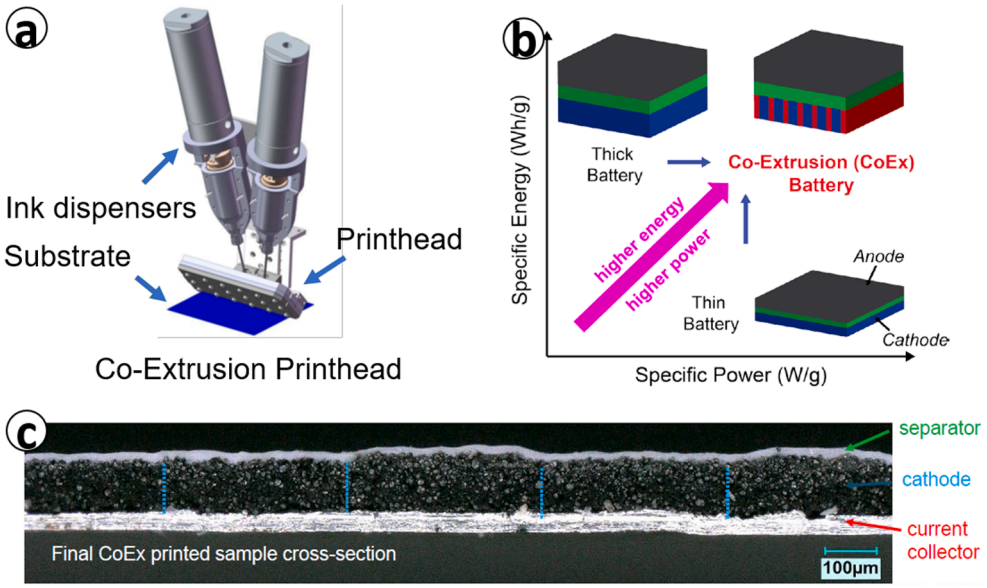

Fig. 3. Co-extrusion was developed to print battery electrodes. (a) Schematic illustration of Co-Extrusion printhead. (b) Co-extrusion of printed battery exhibits a good combination of higher power and higher energy. (c) The cross section of co-extrusion printed cathode [83].

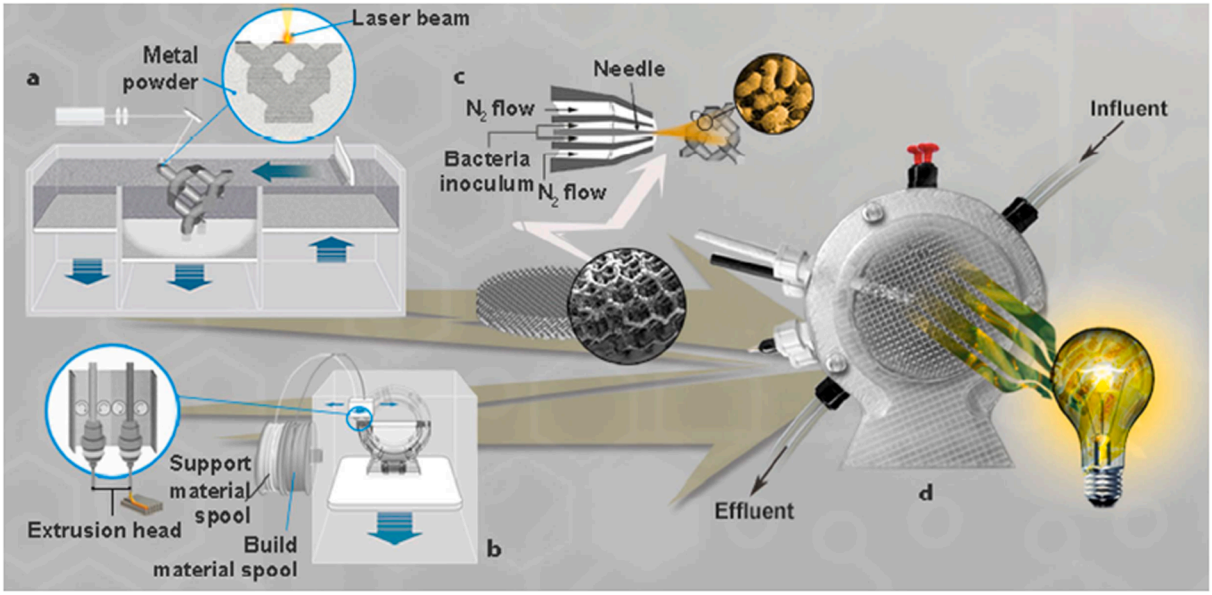

Fig. 4. AM techniques for microbial fuel cells (MFC). (a) Selective laser melting (SLM). (b) Fused deposition modeling (FDM). (c) Anest-Iwata spray gun for bacteria spray-coating. (d) MFC assembly [29].

the GFC cross-sectional dimension ranging from 0.3 to 1.5 mm. Bourell et al. [50] examined laser-sintered graphite BPs and investigated the impact of the carbon fiber content on the strength and electrical conductivity of the printed BPs. In addition, porous media flow field, originally proposed in [96], is adopted in Toyota Mirai fuel cell vehicles (FCV) as their cathode GFCs [97]. Metal/carbon foams with high porosity (>0.9) and permeability, a pore size of ~ 100 μm, adequate thermal/electric conductivity and corrosion resistance of solid matrix, and proper surface wettability are desirable for this new type of distributor [98–100], which can be well controlled during AM processes. As an example, EBM has been employed to fabricate Ti–6Al–4 V open cellular foams [101] and open-cellular copper structures [102]. BOP components in fuel cells, such as cooling units, humidifiers, heat exchanger, and pipe fittings, are 3D printable, and thus their design/prototyping can be facilitated by AM techniques.

Small or tiny PEM fuel cells with an active area less than 1 cm^2, also called micro-fuel cells, have been explored for portable applications. Scotti et al. [103] employed laser AM for the rapid prototyping of stainless-steel micro/mini-size fuel cells, and fabricated three units with various flow fields, including square pillar flow field and inserted carbon cloth. Two additional units with different numbers of channels were fabricated and studied in their following work [104]. Gould et al. [105] employed DMLS to make 21-cm^2 titanium-alloy BPs with flow channels. They indicated that more effort is required to reduce the weight and increase the flatness of BPs for large fuel cell stacks. AM can also be used to print micro/mini-channels in polymer composite plates, which can convert to carbon plates by pyrolysis carbonization for BPs or other carbon-based microfluidics devices [106,107]. Electrolyzers are reverse fuel cells, which produce hydrogen gas through water splitting. Some of their components have been fabricated using AM. Mo et al. [108]

printed perforated Ti plates as the porous transport layer (PTL) using EBM. The pore structures in PTLs with a pore size usually in a range of 20–100 μm play an important role in effective liquid supply and gas removal, which can be designed digitally, and 3D printed precisely. Ambrosi et al. [109] employed SLM and FDM to fabricate metallic electrodes and the liquid/gas handling components for electrolyzers.

3.4. Oil and gas industry

The adoption of AM in the oil and gas industry has been slower in comparison to the aerospace or medical-based industries, however, there is great potential for the use of AM in the industry. In general, the key advantages of AM, such as flexibility in design, the fabrication of complex geometries, consolidation of multipart assemblies into single components, is equally useful for the oil and gas industry [110,111]. AM was used to reduce the multicomponent assembly of a pad scree components to a single part, increasing its effectiveness and decreasing the component lead time; all leading to a reduction in cost by 70%. The current use of AM in this field is primarily applied in the area of rapid prototyping, which in turn is leading to faster product development [112,113], and, in some cases, AM is being used for the development of unique tooling used in the manufacture of end-use parts [114]. Companies such as GE are evaluating the use of AM to print parts for turbine components, centrifugal pumps, and down-hole sensor array housings. The use of AM in this industry is only projected to grow with the potential of generating revenues in the order of $2 billion dollars by 2027 [115]. The real potential for AM will be in increasing the efficiency of the supply chain for the various components needed at onsite facilities. Currently, to minimize the potential of equipment downtime, a high stock of failure-prone components is kept on hand for quick repairs. Additionally, due to the usual remote location of production facilities spread across the world, the supply chain of spare parts is complex. AM's potential to manufacture parts on-demand can facilitate the decentralization of the supply chain, even leading to the manufacture of components onsite as needed and thus eliminating the need for large spare part inventories, which provides significant benefit on cost saving.

4. Challenges of additive manufacturing for energy systems

4.1. Feedstock

The feedstock materials used to generate the final components is important to AM processes. The characteristics of the feedstock materials have a direct effect on the performance of the final manufactured components in the harsh environments in the energy systems. Powder (including powder/liquid slurries), wire, and sheet are the primary forms of feedstock materials for AM processes. Powder-based AM processes, such as PBF or DED, have widely used to fabricate metals and alloys. The current challenges in powder feedstock that can lead to variability in the final AM part include elemental purity, batch-to-batch consistency, the influence of powder production methods, and environmental conditions. Elemental and alloy purity are important in the feedstock to ensure the correct properties are being attained in the printed parts. It has been shown that, despite powders consisting of similar sizes, different batches of AM powder had different flow characteristics [116]. Powder agglomeration or off-spherical shapes could lead to the non-uniform packing or feeding, and thereby the non-uniform powder flowability and the non-uniform microstructure of the AM parts [117]. Furthermore, it was found that a change in the gas used during gas atomization, a typical powder production process, lead to powders of similar compositions being comprised of different phases [118–120]. Environmental influences such as humidity can adversely affect powder characteristics with the potential to induce clumping and thus reducing a powders flowability [119,121]. Moreover, there is a lack of agreed upon methodologies to properly characterize powders for use in the different AM processes. For example, in DED systems, where the powder is taken from a hopper and deposited at the build surface through a carrier gas, the flowability of the powder is important. However, in PBF systems where the powder is spread from a hopper tank across the build plate to create a new layer, the spreadability of the powder is important. Thus, it becomes apparent that the correct powder methodology becomes dependent on the AM process being employed. Traditionally, such information is laid out through some standards, e.g., ASTM. Although ASTM F3049 [122] stipulates powder characterization techniques for AM, it largely points to other ASTM standards that were based on traditional powder metallurgy processes [119,121,123]. There is a need for the continued development of standards on the methods to characterize powder feedstocks, but these will likely need to be AM process specific.

4.2. Dimension accuracy and mechanical integrity of structural components

While there has been much interest in AM across a number of industries, the actual application of the techniques in the manufacturing of structural components in nuclear energy and oil & gas industry has not reached the full potential. This is due in large part to the significant variation seen in AM material properties, causing it to be considered to be less reliable in many cases [124]. This variation in properties ranges from mechanical properties to defects. The surface condition is a key parameter for using components in the as-printed state. In many cases, such as in powder printing, this is not recommended, due to the rough surface caused by partially bonded particles [125]. Printed material roughness is dependent on the AM technique, material, layer thickness, and orientation (surfaces normal to the energy source tend to be rougher). Machining the surface clearly improves the surface roughness and resulting properties [126], and, in many cases, the expectation with the additive techniques is that the component will be made in near-net shape and then machined to the final shape. This removes the concerns of surface condition; however, it also limits the application of AM technology, which promises very complex geometries, which would not be accessible to machining tools. One approach to mitigating this problem is to perform laser surface modification during the build to reduce the initial surface roughness [127].

The use of witness specimens as a means of checking print quality has resulted in a relatively large tensile property database for AM materials. The challenge with this data is the large variation in the results [128,129]. Even in cases of a single test lab within single builds and build-to-build, the tensile properties have been found to have a higher variation for AM material than wrought material [130]. Often yield stress and ultimate tensile stress are higher for AM material as compared to wrought properties, however, total elongation is often lower [128,131]. For any of these properties, however, there are cases where the reverse is true, which is a result of the large scatter in mechanical properties for AM material. This comparison is complicated by the large variations in processing parameters, as well as the data at times representing as-printed material vs heat-treated material. Thermal history during the build also plays a large role in the resulting microstructure and mechanical properties [132]. Heat treatment has a large effect on AM material [132], and, as it is expected that printed material will likely undergo a stress-relaxation heat treatment as a bare minimum, the heat-treated material is generally of more interest. Build orientation has also been observed to affect tensile properties, with the tests performed with the tensile axis perpendicular to the build plane exhibiting poorer tensile properties in general [133]. Hot isostatic pressing (HIP) has been demonstrated to reduce the orientation effect on tensile properties [134].

While tensile tests are typically performed to check AM material quality, recent years have seen an increase in fatigue testing, which is important for nuclear energy and oil & gas applications. Similar to tensile properties, reported fatigue results are incredibly varied [131] and have been found to improve with a HIP treatment following the AM

build [134–136]. AM properties of note that have been reported to affect the fatigue strength of the material include surface condition, build orientation, defects, and process parameters of the AM build. In addition to studies on fatigue life, work has been performed on the effects of AM parameters on crack growth rates as well [137–139]. While not surprising, given the sensitivity of fatigue testing to specimen surface condition, variation has been noted between machined specimens and as-printed specimens, generally in favor of the machined specimens [140]. What is perhaps more surprising is the reports of the small size of this variation, which has been attributed to the presence of large internal flaws, particularly a lack of fusion in the powder and between print layers [141], as well as the machining bringing the voids to the surface, where fatigue cracks tend to initiate [136]. Fusion defects, unlike the spherical voids that may form due to trapped gas, are flat and nearly crack-like. These are typically an indication of incomplete melting and would likely disqualify the material from use, as they significantly degrade the mechanical properties. Reports conflict on whether build orientation has a significant effect on fatigue properties. In some cases, variations in fatigue life and crack growth rate have been observed based on the build orientation, with the specimens tested "vertically", with the build plane normal the tensile axis, exhibiting poorer fatigue properties [133,141]. Other reports have shown that the build orientation had a minimal to zero effect on fatigue properties [142]. The lack of orientation effect was attributed to careful control over-processing parameters that minimized the porosity in the material. Some crack growth behavior differences were observed based on the build-up rate during the build, though primarily in the low stress intensity range near the threshold where cracking was too slow to measure/observe [139]. Given that HIP has generally been shown to improve the mechanical properties of AM material and, in particular, to reduce the variation caused by orientation, it is reasonable to conclude that the presence of voids plays a significant role in both the materials that exhibit poor mechanical properties and the reason behind the strong orientation effect often observed in testing. It has, in fact, been shown that, if fatigue data is correlated to defect size at the location of the crack initiation, the large scatter in fatigue data is drastically reduced [135]. This is likely a result of the voids acting as crack initiation sites.

4.3. High-performance printable batteries

In printed batteries, hermetic sealing can be an issue because it is difficult to keep moisture in the air from permeating into the battery. Some battery chemistries will not work if there is trace water in the electrolyte. With aqueous electrolyte-based battery chemistries, water can permeate out of the cell as well, and that will influence the performance also. The requirements of thin packaging (sometimes optically clear, in which case plastic-aluminum laminates are out of question), abuse tolerance, reduced flammability, and printability put conventional LIB-favorite electrolyte solvent like ethylene carbonate (EC), diethyl carbonate (DEC), dimethyl carbonate (DMC), ethyl-methyl carbonates (EMC), etc. at a disadvantage, as well as $PF6^-$ anion which generates hydrofluoric acid (HF) upon meeting water, which is toxic and corrosive.

For these reasons, instead of carbonate-based liquid electrolytes, most printable battery companies advertise their products as using "solid electrolytes" and therefore are "solid-state battery" which are more abuse-tolerant. These "solid electrolytes" may still have some liquid components inside, but these liquid components are typically more water-tolerant and less volatile, often ionic liquid based (high ionic strength, with large anions) to improve conduction and reduce contact impedance. For example, in Imprint Energy's initial formulation [143], "gel electrolyte is composed of a 1:1 mixture of PVDF-HFP and 0.5 M solution of zinc trifluoromethanesulfonate (Zn^+Tf^-) salt dissolved in $BMIM^+Tf^-$ ionic liquid." [81]

For high-performance batteries where energy and power densities are essential, the "solid-state battery" strategy may not be the right path. But for flexible printable batteries, the total form factor is so small with a smaller number of safety features, the "solid-state" route is unquestionably the right approach. It does come with some sacrifices. Generally, the energy density should be expected to be more than halved compared to state-of-the-art LIB used in cell phones (>270 Wh/kg). The rate capability is negatively impacted as well, as shown in Fig. 16 in Ref. [81]. For a 100 μm-period with 0.98 mAh/cm^2 and 1.2 mWh/cm^2 areal capacities (volumetric energy density is therefore only 120 Wh/L, just ~20% of the state-of-the-art LIB's 700 Wh/L), there is significant drop in discharge capacity when the current density is larger than 1 mA/cm^2, or about 1C rate. Another important thing to note is the increasing internal resistance of batteries with smaller footprint. The internal resistance of a good 18,650 cell (~3Ah capacity) is about 100mΩ when new; when used to near end of life, it rises to 400mΩ. However, small-format batteries can have 10 Ω or even higher internal resistance.

4.4. Cost-effective and durable fuel cells

For PEM fuel cells, cost and durability are the two major barriers to their worldwide deployment. The DOE targets $30/kW in capital cost and the 5000 h lifetime for FCV applications [92,144]. AM techniques show great potential of saving both energy and cost in fabrication in comparison with traditional methods, such as subtractive manufacturing. However, it is challenging to compare with the paper-making, stamping, and molding methods, which are currently considered for the mass production of gas diffusion layer (GDL), BP, and BOPs. For BPs, the DOE 2020 target is $3 per kW or equivalent to two pieces of BPs with each having a ~1000 cm^2 active size and GFCs [144]. Thus, great effects are needed to further reduce AM costs to compete with these traditional fabrication methods for fuel cell mass production. Fuel cell durability is mostly concerned with electrode degradation. However, metallic BP and cooling channels may be subject to corrosion in the fuel cell electrochemical environments or to leakages caused by material deformation or crack formation. To prevent corrosion, AM process needs to be designed and selected to meet the durability requirements. AM components may suffer from residual stress and hole/defect formation, which could cause leakage. In PEM fuel cell, the operating pressure of gaseous reactants such as hydrogen fuel is 2 atm (absolute), thus severe leakage could occur with the presence of very small deformation or cracks. In AM, residual stress arises from temperature gradient during printing processes and is currently an ongoing research needs to be resolved. Gould et al. [105] reported that the flatness of AM fabricated BPs must be further improved for stack applications. Holes, cracks, and other defects may result from gas or impurity being trapped during melt solidification. Those spots are susceptible to corrosion and erosion, causing the leakage of the pressurized gaseous reactants and coolant. These challenges also apply to electrolyzers, which are anticipated to operate under high pressure (e.g. ~ 1 MPa) and for a long duration (e.g. 10–20 years) in order to meet the 2020 DOE cost target of $2.3/kg H_2 [145]. Note that though in general cost-effective and durable AM materials are highly desirable for all the other energy applications, fuel cells require the printed components to meet the specific cost and durability targets, because the cost and durability are widely regarded as the two main barrerites to the commercialization.

5. Fundamental research needs

5.1. In-situ process monitoring

While AM has significant advantages, it also faces the major challenge of achieving the expected quality in material properties. As they stand today, most AM processes are incapable of matching the repeatable quality of traditional manufacturing. This is especially true in the case of thermally-aided AM processes, where the deposition material undergoes a change in its physical phase. Solid materials are heated such that they change phases to liquids, which are then deposited layer-by-

layer and allowed to solidify. After solidification, there is significant reheating as new layers are printed on top of previous layers. Solidification defects, such as micro-cracks, pores, and residual stress, have been reported in the printed structural components. These localized defects could be detrimental to the materials performance under the severe conditions, such as in the nuclear reactor system, batteries, fuel cells, electrolyzers, and offshore environments. Control of the porous architectures in the printed electrodes could lead to higher power efficiency in MFCs [87]. Therefore, it is critical to be able to ensure consistent material addition, microstructure, and properties. In order to address the reliability and consistency issues during AM processing, there are in situ monitoring systems, which commonly employ high-speed cameras [146], near-infrared (NIR) thermal complementary metal-oxide semiconductor (CMOS) cameras [147], pyrometers [148], photodiodes [149], or the combination thereof to assess melt pool and thermal history during processing [150]. Typically, in situ infrared or NIR measurements have been used to monitor melt pool geometry and temperature to predict defects [151]. However, these methods of defect detection require significant integration with machine laser optics and usually require high acquisition rates on the order of 10 kHz to track the highly dynamic temperature fluctuations [152]. Full-field imaging to use lower framerate captures with lesser data storage requirements may require more computation. The associated data processing, highspeed imaging rate, and time-resolved measurements are also critical [153]. The fundamental research needs are apparent to develop precise monitoring systems for AM processes.

5.2. Modeling of AM processes

Modeling is an important aspect in AM development, which improves the understanding of its physical mechanisms and development of optimal strategies in fabrication. It is a powerful tool to address the major concerns, as discussed for AM in energy applications, such as material deformation, cracks, and surface flatness. A recent review was provided for melt-extrusion AM processes [21] and PBF processes [154]. In this section, we focus on the modeling activities primarily associated with laser or electron-beam-based AMs, for which major efforts have been made to formulate the complex heat and transport processes. Table 2 summarizes a few modeling efforts, including finite element modeling, volume of fluids (VOF), Lattice Boltzmann methods (LBM), statistical methods, and molecular dynamics (MD). The major physical phenomena in SEBM/SLM are elucidated in Fig. 5 [154]. The temperature distribution/evolution, molten pool dimension, two-phase flow, rapid phase change, and residual stress are the major targets of AM modeling. In laser-based AM processes, the laser heat addition is assumed to be a moving heating source with a heat flux following the Gaussian distribution:

$$Q_r = \frac{2P}{\pi r_0^2 H}\left(1-\frac{z}{H}\right)\exp\left(1-\left(\frac{r}{r_0}\right)^2\right) \quad (1)$$

where Q_r is the input energy density, P is the absorbed beam power (W), and r_0, H, r, and z are parameters regarding the size and penetration of a laser beam [155,156]. A similar approach was adopted in EBM [157]. The double ellipsoid model, which describes the power distribution in the transverse, depth, and longitudinal dimensions, was also proposed [158,159]. In laser-based AM processes, only about 30–50% of the laser power is absorbed by a molten pool, due to heat loss caused by reflection on deposited metal, absorption by in-flight powders, absorption by material evaporation, and the dependence of surface absorptivity on materials, temperature, and beam wavelength [155,160]. In addition, the molten pool size can vary due to the change of cooling conditions. For example, the substrate base dissipates heat quickly, which yield a small molten pool in the initial layers during fabrication. Strategies, such as tuning the laser power, have been developed to ensure identical molten pool size throughout the entire processes. [155].

Table 2
Examples of modeling efforts in AM.

Authors	Modeling Method	AM Method/ Material	Remarks
Dunbar et al. (2016) [159]	Finite Element Model	LPBF/Inconel® 718	Validate axial distortion in fabricated pipes
Want et al. (2008) [155]	Finite Element Model	LENS/SS410	Validate T distribution in a single wall fabrication. Study cooling rate distribution.
Shen and Chou. (2012) [157]	Finite Element Model	EBAM/ Ti-6Al-4V	Validate T distribution. Study a few configurations of powder layer.
Klassen et al. (2014) [161]	LBM	SEBM/ Ti–6Al–4V	2D LBM. Solve the hydrodynamics and thermodynamics of the molten material. Study penetration depth of the electron beam.
Lee and Zhang (2016) [162]	VOF	L-PBF/ Inconel® 718	Combine a powder packing model based on Discrete Element Method and a 3-D transient heat and fluid flow simulation. Also study the solidification morphology and grain size
Gürtler et al. (2013) [163]	VOF	Laser beam melting/ Steel powders	Study effects of the powder-layer thickness, moving heat source intensity, scan spacing and scanning velocity. Use OpenFoam for 3D VOF.
Tapia et al. (2018) [164]	Statistic Model	L-PBF/SS316L	Use a Gaussian process-based surrogate model to predict melt pool depth given a laser power, scan speed, and laser beam size combination using their and literature data.
Vo and Kim (2017) [165]	MD	SLM/Ag nanocluster	Use LAMMPS for MD. Find the melting point, heat of fusion, entropy of fusion, and surface energy are highly dependent on the nanocluster size in the range of 2.1–6.9 nm in diameter.
Ji et al. (2020) [166]	MD	SLM/AlSi10Mg	Use LAMMPS for MD. Find local thermal gradients cause Si segregation, and the rapid cooling rate leads to a large number of subgrains.

Temperature (T) and its changes are the most important quantities in AM, which determine material properties and final product quality. To predict emperature behaviors, thermal models have been employed to describe the heat transport during fabrication, with an example given as below:

$$\left(\rho C_p\right)^{eff}\frac{\partial T}{\partial t} + \nabla\cdot\left(\rho_l C_{p,l}\mathbf{u}T\right) = \nabla\cdot\left(\lambda^{eff}\nabla T\right) + Q \quad (2)$$

where t is time, ρ the density, C_p the specific heat, λ the thermal conductivity, $\mathbf{u}$ the liquid velocity, and Q the heat source, including the latent heat release/absorption during phase change. Note that density, thermal conductivity, and specific heat are dependent on temperature, material phase, and powder characteristics. The temperature gradients in the molten pool could result in fluid flow due to the temperature dependent surface tension. The induced flow velocity can reach as high as 1 m/s [167], promoting strong convective heat/mass transport. Khairallah et al. [168] presented a 3D mesoscopic model for stainless steel 316 SLM, which couples thermal diffusion with hydrodynamics and takes into account the temperature-dependent material properties, surface tension, and powder size distribution. A monomodal particle size distribution with a mean diameter of 27 μm was assumed to predict the major laser track characteristics.

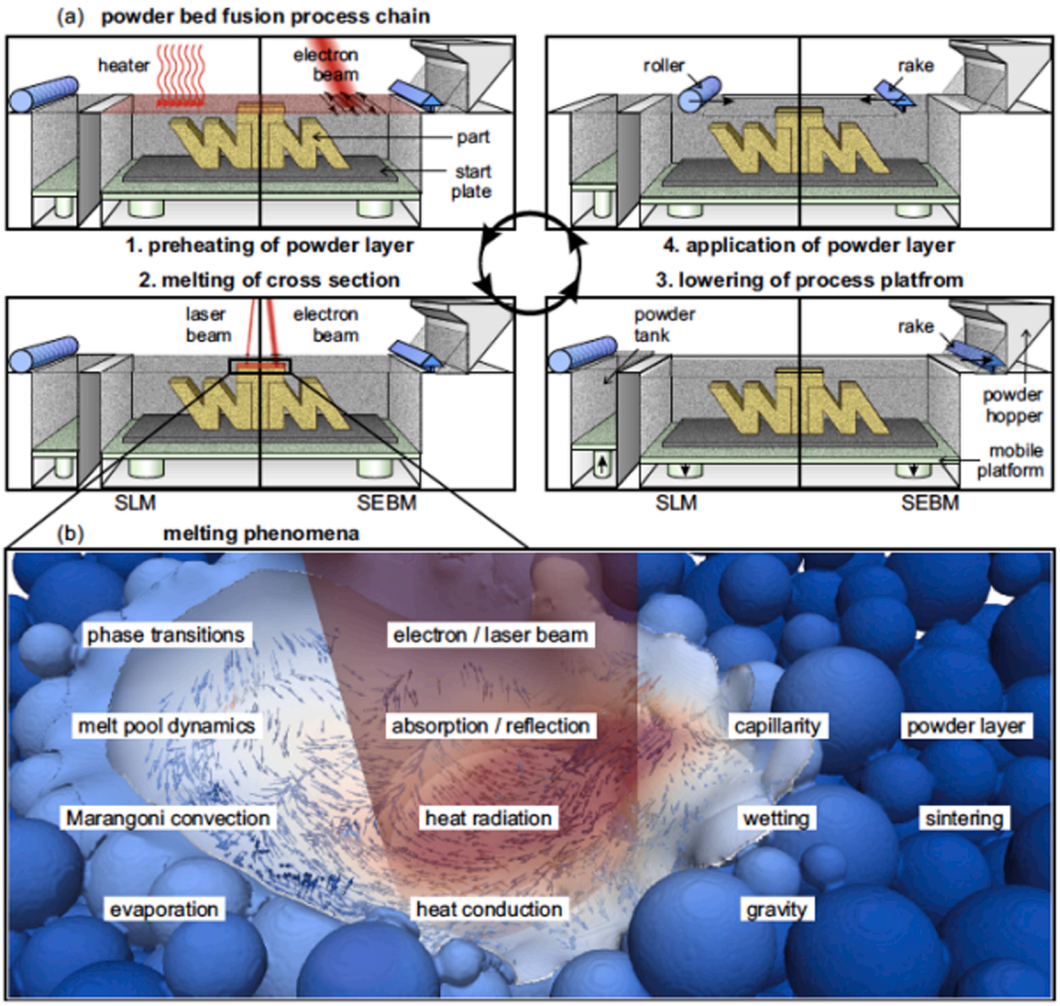

Fig. 5. (a) AM process and physical phenomena in SLM (left) and SEBM (right) and (b) Dominant physical phenomena during melting in a partially molten powder bed [154].

In addition, spatial and temporal temperature variations lead to thermal distortion and consequently materials failure in energy applications, such as the AM components in nuclear power, fuel cells, and electrolyzers. It has been established that thermal distortion is affected by several AM conditions and can be evaluated using strain parameter (ε^*) [167,169]:

$$\varepsilon^* = \frac{\beta \nabla T}{EI} \frac{t}{F\sqrt{\rho}} H^{3/2} \tag{3}$$

where β is the volumetric expansion coefficient, ∇T the difference

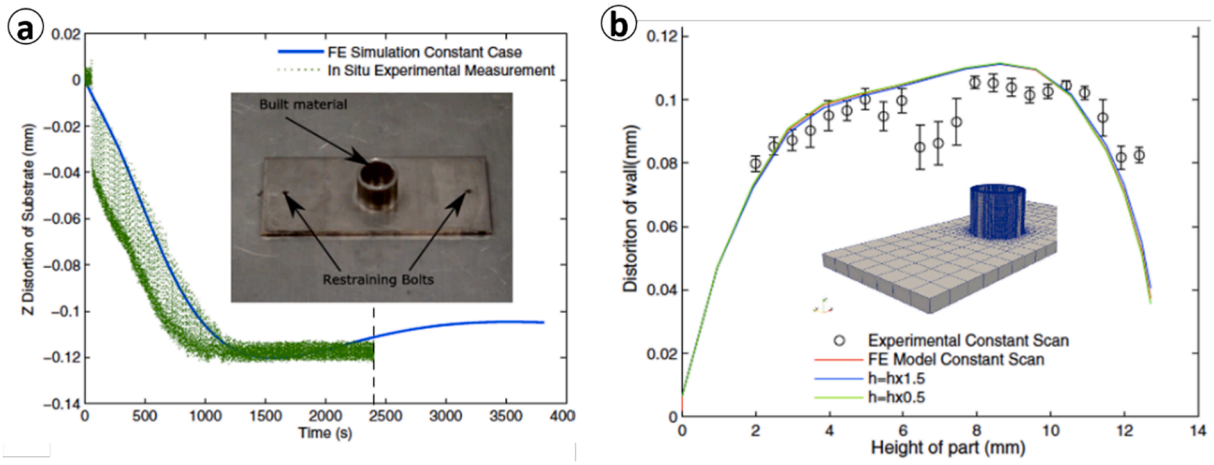

Fig. 6. (a) Comparison of experimental and finite element (FE) model results for distortion of the substrate in the build direction (Z: the axial direction); and (b) sensitivity of post-build distortion to FE model convection coefficient [159].

between the peak and ambient temperatures, t the total AM time, H the heat input per unit length, EI the flexural rigidity of the substrate, F the Fourier number, and ρ is the density of powers. Dunbar et al. [159] carried out both experimental and numerical analysis on Inconel 718 pipes fabricated by laser powder bed fusion. They measured the axial distortion at four locations and compared favorably with their finite element model, in terms of distortion including in-situ data as shown in Fig. 6 (a). They showed that the surface heat transfer coefficient has negligible impact on the distortion, as shown in Fig. 6(b). Note that the level of distortion, ~0.1 mm, as shown in Fig. 6, may lead to severe leakage of pressurized hydrogen reactants in PEM fuel cells and electrolyzers.

As an alternative to physical modeling, statistical methods have been proposed to study AM. Tapia et al. [164] applied a Gaussian process-based surrogate model to predict the melt pool depth in a single-track experiment for a given laser power, scan speed, and laser beam size. 52 data sets of 316L stainless molten pool from [164], 14 from [170], and 73 from the experiment were used to identify the processing windows, within which the molten pool at the laser-powder interface exhibits the desirable thermal conduction mode, as opposed to the keyhole mode.

Two-phase flow dynamics play an important role in AM processes. The formation of cracks or holes reduces the mechanical strength, corrosion resistance, and durability of AM products, which may arise from bubble trapping, impurity evaporation, balling, inadequate liquid imbibition, and undesirable AM planning. Volume of fluid (VOF) methods are widely employed to study two-phase flow, which track the phase interface in computation. In general, VOFs solve the flow equations of each phase, along with a scalar equation of the liquid volume fraction (F) [163,171]:

$$\frac{\partial F}{\partial t} + \nabla\cdot(\mathbf{u}F) = 0 \tag{4}$$

A computational cell is completely filled by liquid when $F = 1$, and is occupied by the other phase when $F = 0$. When F falls between 0 and 1, the cell contains a phase interface. To describe the effect of the surface tension σ at the phase interface, the continuum surface force model is frequently used to add a volumetric force source f_s:

$$f_s = \sigma\kappa\nabla\gamma \tag{5}$$

where $\kappa$is the interface curvature, determined by the unit interface normal $\vec{n}$:

$$\kappa = -\nabla\cdot\vec{n} = -\nabla\cdot\left(\frac{\nabla\gamma}{|\nabla\gamma|}\right) \tag{6}$$

In AM, the molten pool front is an unknown priori and rapidly changes with time, thus, VOFs are suitable to study molten pool dynamics. Lee et al. [172] proposed a VOF study to investigate the effects of laser power, scanning speed, and powder size distribution on the bead geometry and balling defect with individual powder particles resolved using a mesh size of 3 μm. The study showed that balling defects initiate from a void at the center of a molten pool, and, as the void expands, the molten pool breaks apart into separate islands. Gürtler et al. [163] employed the software OpenFOAM to conduct a 3D VOF study on the laser-based AM of steel powders. They tracked the free surface of the molten steel in VOFs and examined the effects of the powder-layer thickness, moving heat-source intensity, scan spacing, and scanning velocity on process dynamics.

Lattice Boltzmann model (LBM) is a numerical method to study the transport and fluid flows, involving interfacial dynamics and complex geometries [173]. It is based on momentum conservation and considers flows to be composed of a collection of pseudo-particles residing on the nodes of a lattice structure. The LBM governing equations are different from the conventional continuum description, such as the Navier–Stokes equations. LBM uses distribution function to represent the probability of finding fluid particles. Comparing with VOF methods, LBMs are advantageous in eliminating explicit interface tracking because of its inherent incorporation of particle interactions to yield phase segregation. Klassen et al. [161] employed a 2D single-phase free-surface LBM method, which takes into account wetting and capillary forces, convective mass and heat transport, and melting and solidification, to investigate the impacts of the electron beam's acceleration voltage on attainable melt depth, mass loss, and recoil due to evaporation, as seen in Fig. 7. The evaporation rate is described by the flux of particles leaving the surface of the condensed phase j^+ and that returning to its surface j^-:

$$j^{net} = j^+ - j^- = \left(\frac{j^+ - j^-}{j^+}\right)\cdot j^+ = \varnothing\cdot j^+ \tag{7}$$

where φ denotes the fraction of the net flux of particles escaping into the half-space. They created processing maps under typical SEBM conditions and concluded that increasing the acceleration voltage from 60 to 120 kV is beneficial to medium atomic number materials, such as titanium and its alloys. In general, LBM can be computationally intensive with difficulty in incorporating temperature-dependent properties such as surface tension, thermal conductivity, and viscosity.

MD simulation, a method based on the classical force-field of atomic interactions, provides an effective way to examine interfacial binding [174] and material properties [165] in AM. The model consists of Newton's equations of motion for each atom and the potential to describe their interaction. Vo and Kim [165] applied the embedded atom method to model the interatomic forces by considering the embedding energy as a function of atomic electron density. They employed the Large-scale Atomic/Molecular Massively Parallel Simulator (LAMMPS), developed by Sandia National Laboratories for MD simulations, and found that the melting point, heat of fusion, entropy of fusion, and surface energy are highly dependent on the Ag nanocluster dimension, ranged from 2.1 to 6.9 nm in diameter. Ji et al.[166] also employed LAMMPS for MD study on SLM of AlSi10Mg to explain the mechanism of forming a unique network-like silicon-rich structure. They showed local thermal gradients causes Si segregation, and the rapid cooling rate lead to a large number of subgrains. The difference in equilibrium electrochemical potential causes galvanic corrosion, and a structure with low work function in the molten pool causes pitting.

Many questions are still open for computational simulation and modeling of AM processes. The underlying physics of microstructural evolution and chemical redistribution in a nonequilibrium state during the AM processes is still not well understood. There are few studies using the powerful tools of VOF and LBM to understand molten pool dynamics by considering all the major physical processes such as heat transfer, temperature-dependent properties, and phase change. MD study is also rare, and yet will be very helpful to study the nonequilibrium state, rapid heating/cooling process, mechanisms of grain and nanostructure formation, molecular binding, and nano-powder behaviors.

5.3. AM materials under extreme environments in energy systems

AM processes provide unique challenges not experienced in traditional manufacturing methods. Due to the nature of many AM processes, it is difficult to control the thermal history of a component, resulting in heterogeneous microstructures and defect distributions [136]. This can be a result of the size of the component, variations in thickness, or the number of components. As microstructure plays a significant role on the material behavior in extreme environments, whether it be mechanical properties or other environmental effects, it is vital that this process be better understood and controlled.

The reliance on witness specimens and printed coupons to determine the results of process parameters is time-consuming and costly, and typically only covers low-temperature applications (witness specimens have not been used for creep or high-temperature cyclic testing). There

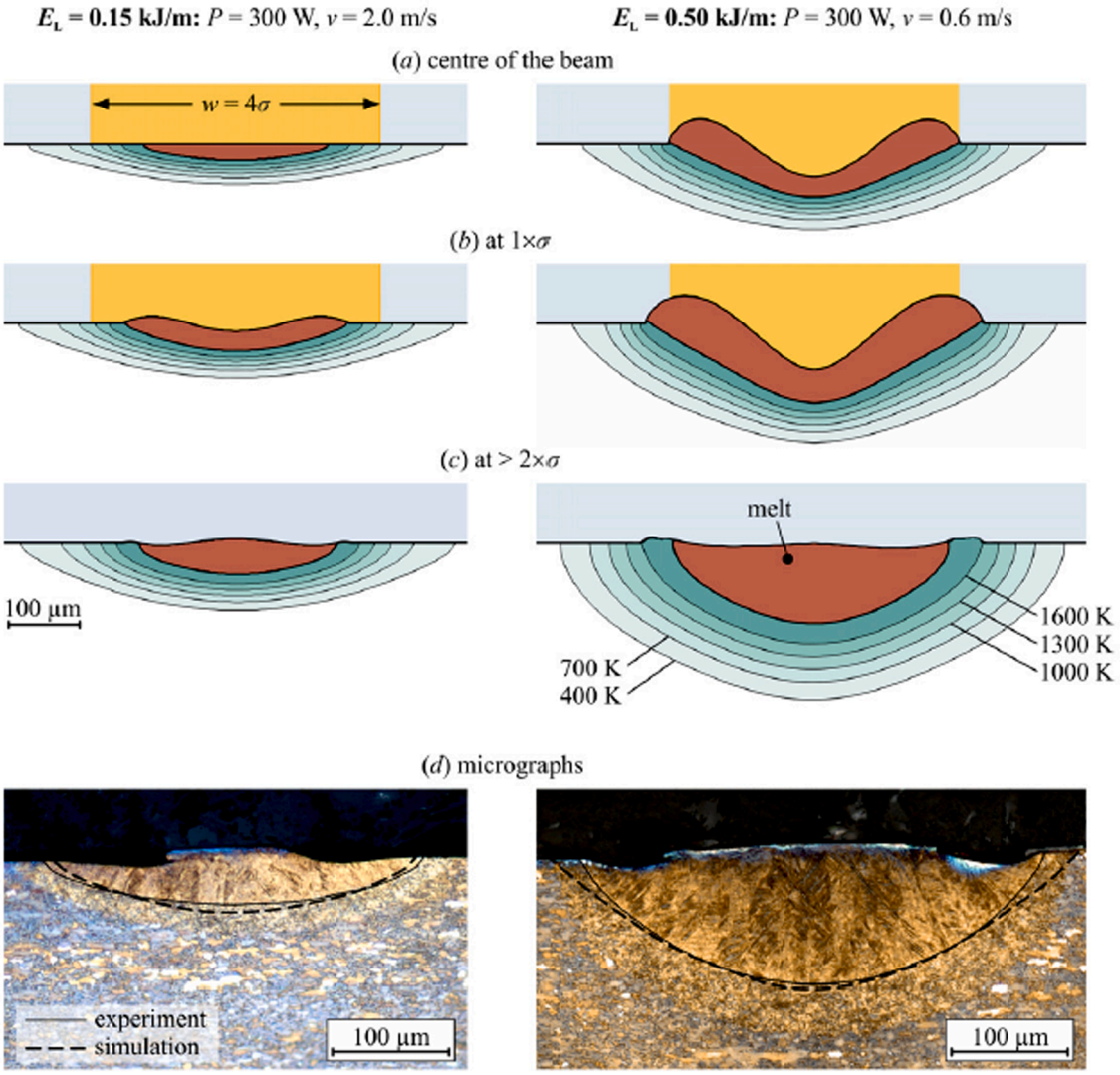

Fig. 7. Single tracks in dense Ti–6Al–4V samples for a 60 kV electron beam (300 W) at different line energies. (a)–(c) LBM-simulated temporal evolution of the melt pool with σ = 100 μm. The spatial resolution is 1 μm. (d) Micrographs of cross-sections of the experimental single tracks, where the molten area is indicated by a solid line and the computed envelope of the melt pool by a broken line [161].

is a large need for better AM models that more accurately reflect actual thermal histories, as well as the resulting variations in microstructures, to reduce the need for experimental optimization of processing parameters. The testing of AM material so far has largely, if not entirely, been performed with uniaxial testing. There is a need to expand this work to examine the effects of multiaxial loading [140], particularly for AM components which have exhibited anisotropic mechanical strengths. While necessary for all testing, it is expected that multiaxial testing would be of particular importance when considering elevated temperature failure mechanisms. While there is an increasing amount of research being performed on the fatigue characteristics of AM material, the most of this work is being performed at or near room temperature. For energy applications, however, there is a need to understand and qualify the behavior of AM materials at elevated temperatures. Long-term and time-dependent failure mechanisms such as creep and creep-fatigue damage control the design of high-temperature structural components. These failure mechanisms are connected to time-dependent properties, such as creep, thermal aging, cyclic softening, etc., and not time independent properties, such as yield stress and ultimate tensile stress. There is a significant gap in understanding the effects of AM properties on the corrosion of a material. For many advanced energy systems, the environments have become increasingly complex (molten salt, liquid sodium, super critical water, and super critical CO_2). For the use of AM within these, and other environments, there needs to be an increased understanding of the corrosion behavior of AM materials.

In recent years, our understanding of the radiation effects on AM components has begun to increase. This is a necessary area of study prior to the use of AM for reactor core and internal components. One aspect of particular importance in light-water reactors is the increased susceptibility to stress corrosion cracking, termed irradiation-assisted stress corrosion cracking (IASCC). Initial results suggest that AM steel show great resistant to IASCC [22,46], as seen in Fig. 8, however, the cause behind this is not well understood, in large part due to the combination of microstructural factors that make AM material distinct from wrought one.

6. Conclusions and future directions

AM shows promising advantages in cheap customization, rapid prototyping and production, the ability to generate gradient or even more complex 3D composition, phase and grain size modulation, certain types of performance enhancement (e.g. radiation swelling), and energy consumption reduction. Advances in AM technologies have already benefited several critical energy sectors. In nuclear energy, AM have

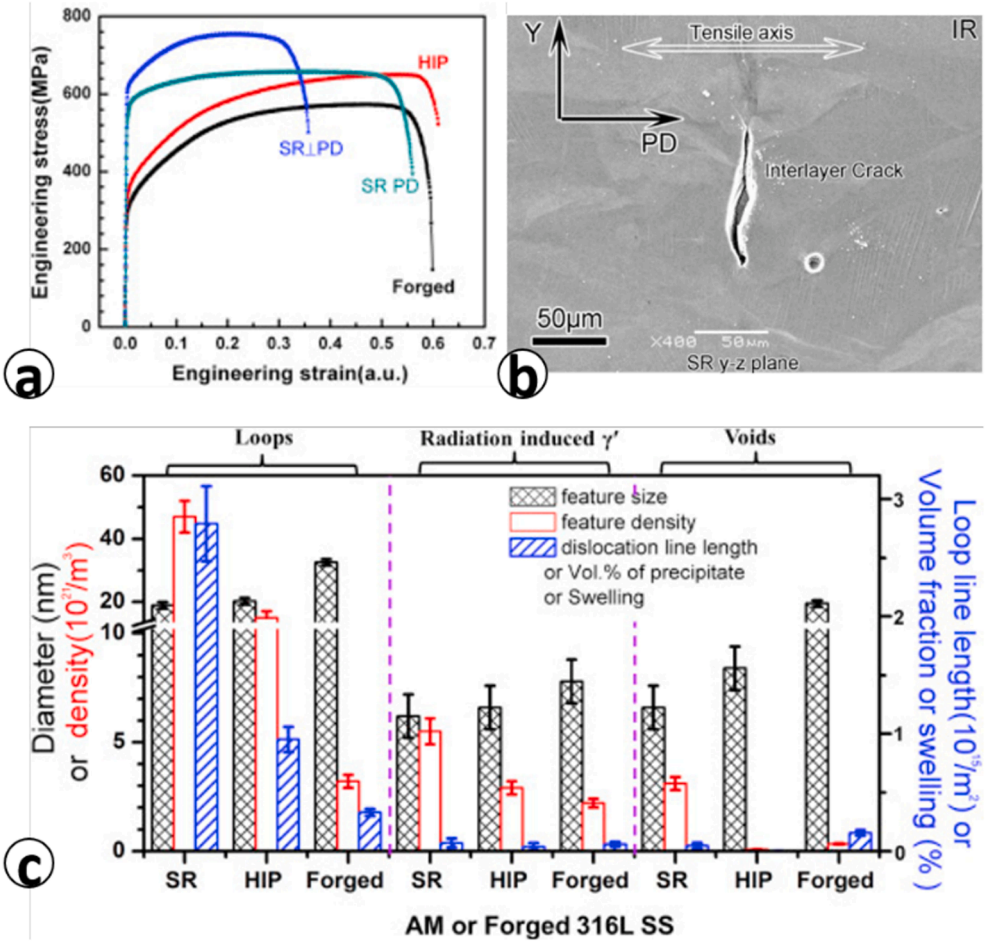

Fig. 8. Irradiation-assisted stress corrosion cracking testing of PBF manufactured 316L stainless steel in a simulated boiling water reactor (BWR) environment. (a) stress–strain curves of 316L stainless steels (SR: printed and stress relieved; PD: printing direction; HIP: hot-isotropic pressed). (b) Grain boundary cracking in the irradiated area of SR specimen under 4% stain along PD. (c) Comparison of irradiation defects in the specimens under proton irradiation [46].

been used to fabricate nuclear core components with improved materials performance in reactor environments. The development of advanced AM technologies could promote the implementation of field-fabrication of nuclear components for advanced reactors, such as small-modular reactors and micro-reactors. The development of sophisticated in-situ monitoring with feedback-control system improves the reliability and consistency of AM processes. With the advances in AM technologies, co-design of printed battery and electronics within one package becomes possible, making smart/IoT devices (such as imbedded sensors) mechanically flexible and autonomous. AM can also simplify the traditional five basic layers of a battery period to three basic layers by merging current collector layer with the adjacent active electrode layer. Co-extrusion is an emerging AM technique that can lay down multi-materials ink in one pass during printing process and the co-extrusion printed battery exhibits a good combination of higher power and higher energy. In fuel cells and electrolyzers, AM processes have been used to fabricate chambers, electrodes, and membranes for MFCs and a whole MFC without bolts or assembling; BPs, porous media flow field plates, cooling units, and BOP components for PEM fuel cells and micro/mini-size fuel cells; and BPs and PTLs for electrolyzers. In addition, AM can handle biocompatible materials, and thus can print batteries and fuel cells for implantable or wearable applications. AM technologies become more and more prevalent in the oil & gas sector with applications, including field manufacturing of components, reducing lifecycle phases of production, prototype design of complex parts, and lowering inventory levels to save costs. The fundamental research on the stability of AM parts used in the extremely hostile downhole environments, including high-pressure, high-temperature, erosion and wear, fatigue and the presence of debris, is essential to the prediction of materials performance and lifetime. Great efforts have been made to understand the fundamentals and underlying physics using advanced computational models. Computational models, such as finite element analysis, statistics formula, VOF methods, LBM models, and atomistic modeling approaches, have been applied to predict temperature distribution and evolution, material distortion, molten pool size and dynamics, and nanocluster-dependent material properties. By tailoring AM parameters, the microstructure and properties of AM components can be tuned to meet the requirement of different energy systems.

Nonetheless, many challenges remain when it comes to the qualification, licensing and manufacturing of commercial products in the energy industry. More research and development are required to overcome the key technical challenges, with great expansion of the AM materials repertoire expected in the future, that will include composites, functional materials, active and biological materials, and embedded micro-nano-devices. We expect that the research and qualification time of AM materials and components to be significantly shorter than the development of traditional manufacturing processes, though, due to the reduced cost and time of producing samples that allows more recipes to tested out, eventually ending up with higher-quality and/or multi-functional products for energy systems.

AM is an important part of lab automation and digital manufacturing. As such, there is a natural synergy between materials design, AM, automated testing, and artificial intelligence (AI) driven

active learning. In the energy systems, the design space of materials and components is often very high dimensional, which includes the base composition, additives, phase and microstructures, gradients, and macro structures (topology optimization) that depends on the processing parameters. A "carpet bombing" approach would be impossible, and historically people have always used intuition and gradients to guide the search for better materials, designs and processes. Humans are also not very good or consistent at repetitive experiments. With lab automation that reduces experimental uncertainty and provides better data provenance, one can use the active learning approach to design and execute the next batch of experiments iteratively, and learn from those results with AI. Gaussian Process (GP) based Bayesian optimization (BO) can drive such active-learning based AM experimentations in high-dimensional design space (as any parametric space dimensions larger than two would quickly become confusing to humans), and will allow automatic decision of the next sets of AM parameters, to optimally balances parameter exploitation, that is the near-term maximization of some figure-of-merit, and exploration, that is the reduction of the Bayesian model uncertainty in a large range of parameter space, not only near the present optimum. To achieve highly efficient active learning and optimization, there needs to be high-throughput, lab-automated characterization and testing that match the throughput of AM. These include sample transfer robots, "self-driving" optical and electron microscopies and spectroscopies, high-throughput mechanical tests, e.g. automated nanoindentation but generalized to tensile tests, automated environmental exposures (e.g. salt-water spray, furnace, electrochemical stability tests), etc.

In the energy industry, refractory metals and ceramics occupy a special place, as higher temperature brings about higher energy efficiency. However, higher temperature service generally brings about higher rate of corrosion as well. For example, AM of refractory body-centered-cubic (BCC) niobium (Nb, density = 8.57 × 103 kg/m3, TMelt = 2750 K), molybdenum (Mo, 10.28 × 103 kg/m3, TMelt = 2896 K), tantalum (Ta, 16.65 × 103 kg/m3, TMelt = 3290 K) and tungsten (W, 19.25 × 103 kg/m3, TMelt = 3695 K) and their alloys would be highly desirable, as theoretically they can have exceptionally slow high-temperature creep rate. However, as of 2019, even with "a special equipment with heating of the substrate plate up to 1273 K, oxygen levels in the process atmosphere below 20 ppmv and a sufficient laser power, Mo and W cannot be processed free of cracks" with selective laser melting AM. The reason is oxidation, as these metals have high solubility of oxygen in the lattice, and oxygen interstitials are highly mobile, so a breach of passivation anywhere on the surface of the component —without a mechanism for self-repair at the location of the breach—would lead to internal oxidation everywhere in the component. In this sense, AM is already be better than bulk casting, as the small melt pool size limits the heat-exposure time and thus oxygen diffusion time compared to bulk casting. Still this is not enough, since the native passivation abilities of refractory Nb, Mo, Ta, W, V elements are all poor. These BCC metals are located quite high on the Ellingham diagram, so their oxides are not as stable as, for instance, Al_2O_3. Cr_2O_3, which otherwise is known as an excellent passivation layer, loses protectiveness at above ~1273 K due to volatilization. Similar volatilization problems exist for Nb_2O_5, MoO_3, WO_3, Ta_2O_5, V_2O_5, etc. Thus, in order to form natural passivation, the addition of non-refractory elements such as Al and Si is necessary. AM would allow gradient distribution of Al substitution or even mixture of Al,Si-bearing phases toward the outer surface, achieving the best tradeoff between defense-in-depth oxidation resistance, and preservation of bulk ductility and creep strength. The addition of Al_2O_3 and carbon nanotubes (CNTs) has been attempted in AM of molybdenum, to promote passivation scale formation [175]. The ability to produce metallic composite powders ~10 μm in size with uniform carbide, oxide, nitride, silicide and boride nano-dispersions inside [176–178] could be essential for such gradient design, and improvement of the creep and radiation resistance of AM high-temperature alloys. More generally, the AM of metallurgical-ceramic composites, fiber–matrix composites, etc. could be highly helpful for improving the thermomechanical stability and other extreme-environment tolerance of the components. Dispersion of externally mixed-in 0D/1D nanocarbides, and in operando formed 0D/2D nano-oxides, is a tried-and-true strategy to mitigate dislocation creep, e.g. in oxide-dispersion-strengthened steels. The AM of these special metal-ceramic composites and their applications in the energy systems could be a hot research area in the future.

Declaration of Competing Interest

The authors declare that they have no known competing financial interests or personal relationships that could have appeared to influence the work reported in this paper.

Acknowledgement

C. S., M. D. M., and N. D. J. are supported by the Idaho National Laboratory Laboratory-Directed Research & Development Program under Department of Energy (DOE) Idaho Operations Office Contract DE-AC07-051D14517. C. S. is also supported by the U.S. DOE, Office of Nuclear Energy under DOE Idaho Operations Office Contract DE-AC07-051D14517 as part of a Nuclear Science User Facilities experiment. Y. W. gratefully acknowledges the support from the U.S. National Science Foundation (NSF) CBET-1336873 on this study. F. L. thanks the sponsor by U.S. NSF CMMI 1625736. J. L. acknowledges the support from the US DOE Office of Nuclear Energy's Nuclear Energy University Program under Grant No. DE-NE0008827. We also thank H. Yuan, B. Zheng. and P. Tian in Y. W.'s group for the assistance in the literature survey and J. Gan, the manager of advanced characterization department at Idaho National Laboratory, for the discussion and review.

References:

[1] Center BP. Annual Energy Outlook; 2012.
[2] Buongiorno J, Corradini M, Parsons J, Petti D. The Future of Nuclear Energy in a Carbon-Constrained World: an interdisciplinary MIT study; 2018.
[3] Nijs JF, Szlufcik J, Poortmans J, Sivoththaman S, Mertens RP. Advanced manufacturing concepts for crystalline silicon solar cells. IEEE Trans Electron Devices 1999;46(10):1948–69.
[4] Post BK, Richardson B, Lind R, Love LJ, Lloyd P, Kunc V, et al. Big area additive manufacturing application in wind turbine molds. Solid Freeform Fabricat Sympos 2017.
[5] Baker J. New technology and possible advances in energy storage. Energy Policy 2008;36(12):4368–73.
[6] Verhoef LA, Budde BW, Chockalingam C, García Nodar B, van Wijk AJM. The effect of additive manufacturing on global energy demand: An assessment using a bottom-up approach. Energy Pol 2018;112:349–60.
[7] https://www.westinghousenuclear.com/about/news/features/view/advancing-our-manufacturing-capabilities-to-meet-your-component-needs.
[8] Hughes JP, dos Santos PL, Down MP, Foster CW, Bonacin JA, Keefe EM, et al. Single step additive manufacturing (3D printing) of electrocatalytic anodes and cathodes for efficient water splitting. Sustain Energy Fuels 2020;4(1):302–11.
[9] https://www.globaldata.com/3d-printing-promises-enhanced-operational-efficiency-and-business-growth-for-the-oil-and-gas-industry-says-globaldata/.
[10] https://www.rigzone.com/news/oil_gas/a/141296/.
[11] Chen K, Huang R, Li Y, Lin S, Zhu W, Tamura N, et al. Rafting-enabled recovery avoids recrystallization in 3D-printing-repaired single-crystal superalloys. Adv Mater 2020;32(12):1907164.
[12] Wrobel R, Scholes B, Hussein A, Law R, Mustaffar A, Reay D. A metal additively manufactured (MAM) heat exchanger for electric motor thermal control on a high-altitude solar aircraft – experimental characterisation. Thermal Sci Eng Progress 2020;19:100629.
[13] Bergeron A, Crigger JB. Early progress on additive manufacturing of nuclear fuel materials. J Nucl Mater 2018;508:344–7.
[14] CW. Current Westinghouse Efforts; 2017.
[15] Pikul JH, Gang Zhang H, Cho J, Braun PV, King WP. High-power lithium ion microbatteries from interdigitated three-dimensional bicontinuous nanoporous electrodes. Nat Commun 2013;4(1):1732.
[16] You J, Preen RJ, Bull L, Greenman J, Ieropoulos I. 3D printed components of microbial fuel cells: towards monolithic microbial fuel cell fabrication using additive layer manufacturing. Sustain Energy Technol Assess 2017;19:94–101.
[17] https://www.metal-am.com/metal-additive-manufacturing-for-oil-and-gas-sector/.
[18] https://www.engineering.com/3DPrinting/3DPrintingArticles/ArticleID/9696/GE-Oil-Gas-Uses-3D-Printing-to-Produce-Control-Valve-Parts.aspx.

[19] Dass A, Moridi A. State of the art in directed energy deposition: from additive manufacturing to materials design. Coatings 2019;9(7):418.
[20] Bhavar V, Kattire P, Patil V, Khot S, Gujar K, Singh R. A review on powder bed fusion technology of metal additive manufacturing. In: Additive Manufacturing Handbook. CRC Press; 2017. p. 251–3.
[21] Turner BN, Strong R, Gold SA. A review of melt extrusion additive manufacturing processes: I. Process design and modeling. Rapid Prototyping Journal 2014.
[22] McMurtrey MD, O'Brien R, Sun C, Shiau C, Teng F. Irradiation damage and IASCC of printed 316L for use as fuel cladding. Proceedings of the 19th International Conference on Environmental Degradation of Materials in Nuclear Power Systems-Water Reactors. 2019.
[23] Kunce I, Polanski M, Bystrzycki J. Structure and hydrogen storage properties of a high entropy ZrTiVCrFeNi alloy synthesized using Laser Engineered Net Shaping (LENS). Int J Hydrogen Energy 2013;38(27):12180–9.
[24] Joseph J, Jarvis T, Wu X, Stanford N, Hodgson P, Fabijanic DM. Comparative study of the microstructures and mechanical properties of direct laser fabricated and arc-melted AlxCoCrFeNi high entropy alloys. Mater Sci Eng A 2015;633:184–93.
[25] Chao Q, Guo T, Jarvis T, Wu X, Hodgson P, Fabijanic D. Direct laser deposition cladding of AlxCoCrFeNi high entropy alloys on a high-temperature stainless steel. Surf Coat Technol 2017;332:440–51.
[26] Wang R, Zhang K, Davies C, Wu X. Evolution of microstructure, mechanical and corrosion properties of AlCoCrFeNi high-entropy alloy prepared by direct laser fabrication. J Alloy Compd 2017;694:971–81.
[27] King WE, Anderson AT, Ferencz RM, Hodge NE, Kamath C, Khairallah SA, et al. Laser powder bed fusion additive manufacturing of metals; physics, computational, and materials challenges. Appl Phys Rev 2015;2(4):041304.
[28] Zhong Y, Rännar L-E, Liu L, Koptyug A, Wikman S, Olsen J, et al. Additive manufacturing of 316L stainless steel by electron beam melting for nuclear fusion applications. J Nucl Mater 2017;486:234–45.
[29] Calignano F, Tommasi T, Manfredi D, Chiolerio A. Additive manufacturing of a microbial fuel cell—a detailed study. Sci Rep 2015;5(1):1–10.
[30] Li L, Bellehumeur C, Gu P. Composite modeling and analysis of FDM prototypes for design and fabrication of functionally graded parts 187. 2001 International Solid Freeform Fabrication Symposium. 2001.
[31] Lacey SD, Kirsch DJ, Li Y, Morgenstern JT, Zarket BC, Yao Y, et al. Extrusion-based 3D printing of hierarchically porous advanced battery electrodes. Adv Mater 2018;30(12):1705651.
[32] Maurel A, Courty M, Fleutot B, Tortajada H, Prashantha K, Armand M, et al. Highly loaded graphite-polylactic acid composite-based filaments for lithium-ion battery three-dimensional printing. Chem Mater 2018;30(21):7484–93.
[33] Wang Y, Chen C, Xie H, Gao T, Yao Y, Pastel G, et al. 3D-printed all-fiber Li-ion battery toward wearable energy storage. Adv Funct Mater 2017;27(43):1703140.
[34] Rao R, Solberg S, Murphy K, Wood M, Li J, Pandey R et al. Thick Co-Extruded Cathode Electrodes for High Energy Lithium-Ion Batteries. Conference: 2018 MRS Fall Meeting & Exhibit; Boston, MA; November 25-30, 2018. 2018. Palo Alto Research Center. Medium: ED.
[35] Shen K, Mei H, Li B, Ding J, Yang S. 3D printing sulfur copolymer-graphene architectures for Li-S batteries. Adv Energy Mater 2018;8(4):1701527.
[36] Gibson I, Rosen D, Stucker B. Vat photopolymerization processes. In: Additive Manufacturing Technologies. Springer; 2015. p. 63–106.
[37] Au AK, Lee W, Folch A. Mail-order microfluidics: evaluation of stereolithography for the production of microfluidic devices. Lab Chip 2014;14(7):1294–301.
[38] Wei L, Zhang J, Yu F, Zhang W, Meng X, Yang N, et al. A novel fabrication of yttria-stabilized-zirconia dense electrolyte for solid oxide fuel cells by 3D printing technique. Int J Hydrogen Energy 2019;44(12):6182–91.
[39] Singh R. Process capability study of polyjet printing for plastic components. J Mech Sci Technol 2011;25(4):1011–5.
[40] Lawes S, Sun Q, Lushington A, Xiao B, Liu Y, Sun X. Inkjet-printed silicon as high performance anodes for Li-ion batteries. Nano Energy 2017;36:313–21.
[41] Huang J, Yang J, Li W, Cai W, Jiang Z. Electrochemical properties of LiCoO2 thin film electrode prepared by ink-jet printing technique. Thin Solid Films 2008;516(10):3314–9.
[42] Ziaee M, Crane NB. Binder jetting: a review of process, materials, and methods. Addit Manuf 2019;28:781–801.
[43] Manogharan G, Kioko M, Linkous C. Binder jetting: a novel solid oxide fuel-cell fabrication process and evaluation. JOM 2015;67(3):660–7.
[44] Jinoop AN, Paul CP, Mishra SK, Bindra KS. Laser Additive Manufacturing using directed energy deposition of Inconel-718 wall structures with tailored characteristics. Vacuum 2019;166:270–8.
[45] Arkhurst BM, Park J-J, Lee C-H, Kim JH. Direct laser deposition of 14Cr oxide dispersion strengthened steel powders using Y2O3 and HfO2 dispersoids. Korean J. Met. Mater. 2017;55(8):550–8.
[46] Song M, Wang M, Lou X, Rebak RB, Was GS. Radiation damage and irradiation-assisted stress corrosion cracking of additively manufactured 316L stainless steels. J Nucl Mater 2019;513:33–44.
[47] Lou X, Song M, Emigh PW, Othon MA, Andresen PL. On the stress corrosion crack growth behaviour in high temperature water of 316L stainless steel made by laser powder bed fusion additive manufacturing. Corros Sci 2017;128:140–53.
[48] Irrinki H, Harper T, Badwe S, Stitzel J, Gulsoy O, Gupta G, et al. Effects of powder characteristics and processing conditions on the corrosion performance of 17–4 PH stainless steel fabricated by laser-powder bed fusion. Progress Additive Manufact 2018;3(1):39–49.
[49] Uddin SZ, Murr LE, Terrazas CA, Morton P, Roberson DA, Wicker RB. Processing and characterization of crack-free aluminum 6061 using high-temperature heating in laser powder bed fusion additive manufacturing. Addit Manuf 2018;22:405–15.
[50] Bourell DL, Leu M-C, Chakravarthy K, Guo N, Alayavalli K. Graphite-based indirect laser sintered fuel cell bipolar plates containing carbon fiber additions. CIRP Ann 2011;60(1):275–8.
[51] Guo N, Leu MC. Effect of different graphite materials on the electrical conductivity and flexural strength of bipolar plates fabricated using selective laser sintering. Int J Hydrogen Energy 2012;37(4):3558–66.
[52] Farandos NM, Kleiminger L, Li T, Hankin A, Kelsall GH. Three-dimensional inkjet printed solid oxide electrochemical reactors I. Yttria-stabilized Zirconia Electrolyte. Electrochimica Acta 2016;213:324–31.
[53] Shallan AI, Smejkal P, Corban M, Guijt RM, Breadmore MC. Cost-effective three-dimensional printing of visibly transparent microchips within minutes. Anal Chem 2014;86(6):3124–30.
[54] Cohen E, Menkin S, Lifshits M, Kamir Y, Gladkich A, Kosa G, et al. Novel rechargeable 3D-microbatteries on 3D-printed-polymer substrates: feasibility study. Electrochim Acta 2018;265:690–701.
[55] Lou X, Gandy D. Advanced manufacturing for nuclear energy. JOM 2019;71(8):2834–6.
[56] Office of Nuclear Energy: 4 Major Opportunities for Additive Manufacturing in Nuclear Energy; 2019.
[57] Terrani K. Advanced Manufacturing and Materials to Enable Advanced Nuclear Energy. In: Transactions of the American Nuclear Society. Philadelphia; 2018.
[58] Hinojos A, Mireles J, Reichardt A, Frigola P, Hosemann P, Murr L, et al. Joining of Inconel 718 and 316 stainless steel using electron beam. Mater Des 2016;94:17–27.
[59] Chen Y, Liou F. Additive manufacturing of metal functionally graded materials: a review. In: Solid Freeform Fabrication 2019: Proceedings of the 29th Annual International Solid Freeform Fabrication Symposium; 2018.
[60] Liu W, DuPont JN. Fabrication of functionally graded TiC/Ti composites by laser engineered net shaping. Script Materialia 2003;48:1337–42.
[61] Carroll BE, Otis RA, Borgonia JP, Suh J-O, Dillon RP, Shapiro AA, et al. Functionally graded material of 304L stainless steel and inconel 625 fabricated by directed energy deposition: Characterization and thermodynamic modeling. Acta Mater 2016;108:46–54.
[62] Bobbio LD, Bocklund B, Otis R, Borgonia JP, Dillon RP, Sapiro AA, et al. Characterization of a functionally graded material of Ti-6Al-4V to 304L stainless steel with an intermediate V section. J Alloy Compd 2018;742:1031–6.
[63] Noecker F, Dupont J. Functionally graded copper - steel using laser engineered net shaping process. In: 21st International Congress on Applications of Lasers and Electro-Optics, Congress Proceedings; 2002.
[64] Jacson TR, Liu H, Patrickalakis NM, Sachs EM, Cima MJ. Modelling and designing functionally graded material components for fabrication with local composition control. Mater Des 1999;20(2–3):63–75.
[65] Wang S, Chen C-S, Zhu Y, Zhu X. Digital design for functionally graded materil components rapid prototyping manufacturing. Adv Geometric Model Process 2008:491–7.
[66] Markworth AJ, Ramesh KS, Parks Jr WP. Modelling studies applied to functionally graded materials. J Mater Sci 1995;30:2183–93.
[67] https://www.energy.gov/ne/nuclear-energy-enabling-technologies/reactor-materials.
[68] https://www.sbir.gov/sbirsearch/detail/1332851.
[69] NUREG/CP-0310 Proceedings of the Public Meeting on Additive Manufacturing for Reactor Materials and Components; 2019.
[70] Terrani K, Kiggans J, Sridharan N, Gussev M, Norfolk M, Burns J, et al. Additive manufacturing of research reactor control elements and subsequent neutron irradiation. Transactions of the American Nuclear Society. 2016.
[71] Burns JR, Chandler D, Petrovic B, Terrani KA. Depletion and lifetime performance analysis of advanced manufactured control elements in the High Flux Isotope Reactor (HFIR). The International Congress on Advances in Nuclear Power Plants. 2018.
[72] Rosales J, Van Rooyen I, Parga C. Characterizing surrogates to develop an additive manufacturing process for U3Si2 nuclear fuel. J Nucl Mater 2019;518:117–28.
[73] Gelis A, Kozak P, Breshears A, Brown MA, Launiere C, Campbell E, et al. Closing the nuclear fuel cycle with a simplified minor actinide lanthanide separation process (ALSEP) and additive manufacturing. Sci Rep 2019;9.
[74] Braam K, Subramanian V. A stencil printed, high energy density silver oxide battery using a novel photopolymerizable poly(acrylic acid) separator. Adv Mater 2015;27(4):689–94.
[75] Cobb CL, Ho CC. Additive manufacturing: rethinking battery design. Electrochem Soc Interface 2016;25:75–8.
[76] Wang Z, Winslow R, Madan D, Wright PK, Evans JW, Keif M et al. Development of MnO2 cathode inks for flexographically printed rechargeable zinc-based battery. J Power Sour 2014;268(Supplement C): 246–254.
[77] Hu L, Wu H, La Mantia F, Yang Y, Cui Y. Thin, flexible secondary Li-ion paper batteries. ACS Nano 2010;4(10):5843–8.
[78] Kohlmeyer RR, Blake AJ, Hardin JO, Carmona EA, Carpena-Nunez J, Maruyama B, et al. Composite batteries: a simple yet universal approach to 3D printable lithium-ion battery electrodes. J Mater Chem A 2016;4(43):16856–64.
[79] Blake AJ, Kohlmeyer RR, Hardin JO, Carmona EA, Maruyama B, Berrigan JD et al. 3D Printable Ceramic–Polymer Electrolytes for Flexible High-Performance Li-Ion Batteries with Enhanced Thermal Stability. Adv Energy Mater 2017;7(14):1602920-n/a.

[80] Mutiso RM, Sherrott MC, Li J, Winey KI. Simulations and generalized model of the effect of filler size dispersity on electrical percolation in rod networks. Phys. Rev. B 2012;86(21):214306.
[81] Ho CC, Evans JW, Wright PK. Direct write dispenser printing of a zinc microbattery with an ionic liquid gel electrolyte. J Micromech Microeng 2010;20 (10):104009.
[82] Blake AJ, Kohlmeyer RR, Drummy LF, Gutiérrez-Kolar JS, Carpena-Núñez J, Maruyama B, et al. Creasable batteries: understanding failure modes through dynamic electrochemical mechanical testing. ACS Appl Mater Interfaces 2016;8 (8):5196–204.
[83] Cobb CL. Co-Extrusion: Advanced Manufacturing for Energy Devices. 2016, PARC, Palo Alto, CA (United States).
[84] Philamore H, Rossiter J, Walters P, Winfield J, Ieropoulos I. Cast and 3D printed ion exchange membranes for monolithic microbial fuel cell fabrication. J Power Sources 2015;289:91–9.
[85] Chaudhuri SK, Lovley DR. Electricity generation by direct oxidation of glucose in mediatorless microbial fuel cells. Nat Biotechnol 2003;21(10):1229–32.
[86] Theodosiou P, Greenman J, Ieropoulos I. Towards monolithically printed Mfcs: development of a 3d-printable membrane electrode assembly (mea). Int J Hydrogen Energy 2019;44(9):4450–62.
[87] Bian B, Wang C, Hu M, Yang Z, Cai X, Shi D, et al. Application of 3D printed porous copper anode in microbial fuel cells. Front Energy Res 2018;6:50.
[88] Zawadzki D, Pędziwiatr P, Michalska K. A novel microbial fuel cell with exchangable membrane-application of additive manufacturing technology for device fabrication. Acta Innovat 2018.
[89] Liu X, Yuk H, Lin S, Parada GA, Tang TC, Tham E, et al. 3D printing of living responsive materials and devices. Adv Mater 2018;30(4):1704821.
[90] Gonzalez-Solino C, Lorenzo MD. Enzymatic fuel cells: towards self-powered implantable and wearable diagnostics. Biosensors 2018;8(1):11.
[91] Du Toit H, Di Lorenzo M. Continuous power generation from glucose with two different miniature flow-through enzymatic biofuel cells. Biosens Bioelectron 2015;69:199–205.
[92] Wang Y, Chen KS, Mishler J, Cho SC, Adroher XC. A review of polymer electrolyte membrane fuel cells: Technology, applications, and needs on fundamental research. Appl Energy 2011;88(4):981–1007.
[93] Chen S, Murphy J, Herlehy J, Bourell DL, Wood KL. Development of SLS fuel cell current collectors. Rapid Prototyping J 2006.
[94] Alayavalli K, Bourell DL. Fabrication of modified graphite bipolar plates by indirect selective laser sintering (SLS) for direct methanol fuel cells. Rapid Prototyping J 2010.
[95] Niemöller A, Jakes P, Kayser S, Lin Y, Lehnert W, Granwehr J. 3D printed sample holder for in-operando EPR spectroscopy on high temperature polymer electrolyte fuel cells. J Magn Reson 2016;269:157–61.
[96] Wang Y. Porous-media flow fields for polymer electrolyte fuel cells. J Electrochem Soc 2009;156(10):B1124.
[97] Yoshida T, Kojima K. Toyota MIRAI fuel cell vehicle and progress toward a future hydrogen society. Electrochem Soc Interface 2015;24(2):45.
[98] Wang Y. Porous-media flow fields for polymer electrolyte fuel cells II. Analysis of channel two-phase flow. J Electrochem Soc 2009;156(10):B1134–41.
[99] Afshari E, Mosharaf-Dehkordi M, Rajabian H. An investigation of the PEM fuel cells performance with partially restricted cathode flow channels and metal foam as a flow distributor. Energy 2017;118:705–15.
[100] Park JE, Hwang W, Lim MS, Kim S, Ahn C-Y, Kim O-H, et al. Achieving breakthrough performance caused by optimized metal foam flow field in fuel cells. Int J Hydrogen Energy 2019;44(39):22074–84.
[101] Murr L, Gaytan S, Medina F, Martinez E, Martinez J, Hernandez D, et al. Characterization of Ti–6Al–4V open cellular foams fabricated by additive manufacturing using electron beam melting. Mater Sci Eng, A 2010;527(7–8): 1861–8.
[102] Ramirez D, Murr L, Li S, Tian Y, Martinez E, Martinez J, et al. Open-cellular copper structures fabricated by additive manufacturing using electron beam melting. Mater Sci Eng A 2011;528(16–17):5379–86.
[103] Scotti G, Matilainen V, Kanninen P, Piili H, Salminen A, Kallio T, et al. Laser additive manufacturing of stainless steel micro fuel cells. J Power Sources 2014; 272:356–61.
[104] Scotti G, Kanninen P, Matilainen V-P, Salminen A, Kallio T. Stainless steel micro fuel cells with enclosed channels by laser additive manufacturing. Energy 2016; 106:475–81.
[105] Gould BD, Rodgers JA, Schuette M, Bethune K, Louis S, Rocheleau R, et al. Performance and limitations of 3D-printed bipolar plates in fuel cells. ECS J Solid State Sci Technol 2015;4(4):P3063–8.
[106] Wang Y, Pham L, de Vasconcellos GPS, Madou M. Fabrication and characterization of micro PEM fuel cells using pyrolyzed carbon current collector plates. J Power Sources 2010;195(15):4796–803.
[107] Jiang S, Shi T, Zhan X, Xi S, Long H, Gong B, et al. Scalable fabrication of carbon-based MEMS/NEMS and their applications: a review. J Micromech Microeng 2015;25(11):113001.
[108] Mo J, Dehoff RR, Peter WH, Toops TJ, Green Jr JB, Zhang F-Y. Additive manufacturing of liquid/gas diffusion layers for low-cost and high-efficiency hydrogen production. Int J Hydrogen Energy 2016;41(4):3128–35.
[109] Ambrosi A, Pumera M. Multimaterial 3D-printed water electrolyzer with earth-abundant electrodeposited catalysts. ACS Sustain Chem Eng 2018;6(12): 16968–75.
[110] Burns M, Wangenheim C. Metal 3D Printing Applications in the Oil & Gas Industry, in SPE Middle East Oil and Gas Show and Conference. 2019, Society of Petroleum Engineers: Manama, Bahrain. p. 9.
[111] Sireesha M, Lee J, Kranthi Kiran AS, Babu VJ, Kee BBT, Ramakrishna S. A review on additive manufacturing and its way into the oil and gas industry. RSC Ad 2018; 8(40):22460–8.
[112] Camisa JA, Verma V, Marler DO, Madlinger A. Additive Manufacturing and 3D Printing for Oil and Gas - Transformative Potential and Technology Constraints. In: The Twenty-fourth International Ocean and Polar Engineering Conference. 2014, International Society of Offshore and Polar Engineers: Busan, Korea. p. 8.
[113] Jacobs T. 3D printing in the oil field kicks into production mode. J Petrol Technol 2016;68(08):30–5.
[114] Vendra L, Achanta A. METAL additive manufacturing in the oil and gas industry.
[115] Additive manufacturing opportunities in oil and gas markets – an opportunity analysis and ten-year forecast. SMARTECH Publishing, 2017.
[116] Lyckfeldt O. Powder rheology of steel powders for additive manufacturing. In: International Powder Metallurgy Congress and Exhibition, Euro PM 2013; 2013. European Powder Metallurgy Association (EPMA).
[117] Anderson IE, White EMH, Dehoff R. Feedstock powder processing research needs for additive manufacturing development. Curr Opin Solid State Mater Sci 2018;22 (1):8–15.
[118] Tan JH, Wong WLE, Dalgarno KW. An overview of powder granulometry on feedstock and part performance in the selective laser melting process. Addit Manuf 2017;18:228–55.
[119] Slotwinski JA, Garboczi EJ. Metrology needs for metal additive manufacturing powders. Jom 2015;67(3):538–43.
[120] Rafi HK, Karthik N, Starr TL, Stucker BE. Mechanical property evaluation of Ti-6Al-4V parts made using electron beam melting. In: Proceedings of the Solid Freeform Fabrication Symposium; 2012.
[121] Snow Z, Martukanitz R, Joshi S. On the development of powder spreadability metrics and feedstock requirements for powder bed fusion additive manufacturing. Addit Manuf 2019;28:78–86.
[122] Powders M, Flowmeter H, Spectrometry F. Standard guide for characterizing properties of metal powders used for additive manufacturing processes. ASTM Int: F3049-14. ASTM International 2014:1.
[123] Spierings AB, Voegtlin M, Bauer T, Wegener K. Powder flowability characterisation methodology for powder-bed-based metal additive manufacturing. Progr Addit Manufact 2016;1(1–2):9–20.
[124] Daniewicz SR, Shamsaei N. An introduction to the fatigue and fracture behavior of additive manufactured parts. Int J Fatigue 2017;94:167.
[125] Strano G, Hao L, Everson RM, Evans KE. Sufrace roughness analysis, modelling and prediction in laser melting. J Mater Process Technol 2013;213:589–97.
[126] Brinksmeier E, Levy G, Meyer D, Spierings AB. Surface integrity of selective-laser melted components. CIRP Annals – Manufact Technol 2010;59:601–6.
[127] Alfieri V, Argenio P, Caiazzo F, Sergi V. Reduction of surface roughness by means of laser processing over additive manufacturing metal parts. Material 2017;10.
[128] Ahuja B, Schaub A, Junker D, Karg M, Tenner F, Plettke R, et al. A round robin study for laser beam melting in a metal powder bed. S Afr J Ind Eng 2016;27(2): 30–42.
[129] Guo N, Leu MC. Additive manufacturing: technology, applications and research needs. Front Mech Eng 2013;8(3):215–43.
[130] Luecke WE, Slotwinski JA. Mechanical properties of austenitic stainless steel made by additive manufacturing. J Res Nat Inst Stand Technol 2014;119: 398–418.
[131] Shamsaei N, Yadollahi A, Bian L, Thomspon SM. An overview of Direct Laser Deposition for additive manufacturing; Part II: Mechanical behavior, process parameter optimization and control. Addit Manuf 2015;8:12–35.
[132] Yadollahi A, Shamsaei N, Thompson SM, Seely DW. Effects of process time interval and heat treatment on mechanical and microstructural properties of direct laser deposited 316L stainless steel. Mater Sci Eng A 2015;644:171–83.
[133] Yadollahi A, Shamsaei N, Thmopson SM, Elwany A, Bian L. Effects of building orientation and heat treatment on fatigue behavior of selective laser melted 17–4 PH stainless steel. Int J Fatigue 2017;94:218–35.
[134] Kobryn PA, Semiatin SL. Mechanical properties of laser-deposited Ti-6Al-4V. Solid Freeform Fabrication Proceedings 2001.
[135] Baretta S, Romano S. A comparison of fatigue strength sensitivity to defects for materials manufactured by AM or traditional processes. Int J Fatigue 2017;94: 178–91.
[136] Yadollahi A, Shamsaei N. Additive manufacturing of fatigue resistant materials: challenges and opportunities. Int J Fatigue 2017;98:14–31.
[137] Nezhadfar PD, Burford E, Anderson-Wedge K, Zhang B, Shao S, Daniewicz SR, et al. Fatigue crack growth behavior of additively manufactured 17–4 PH stainless steel: effects of build orientation and microstructure. Int J Fatigue 2019;123: 168–79.
[138] Riemer A, Richard HA, Brüggemann JP, Wesendahl JN. Fatigue crack growth in additive manufactured products. Frattura ed Integrità Strutturale 2015;34: 437–46.
[139] Riemer A, Richard HA. Crack propagation in additive manufactured materials and structures. Procedia Struct Integrity 2016;2:1229–36.
[140] Afkhami S, Dabiri M, Alavi SH, Bjork T, Salminen A. Fatigue characteristics of steels manufactured by selective laser melting. Int J Fatigue 2019;122:72–83.
[141] Shrestha R, Simsiriwong J, Shamsaei N. Fatigue behavior of additive manufactured 316L stainless steel parts: effects of layer orientation and surface roughness. Addit Manuf 2019;28:23–38.
[142] Torries B, Shamsaei N, Thompson S. Effect of build orientation on fatigue performance of Ti-6Al-4V parts fabricated via laser-based powder bed fusion. In: Solid Freeform Fabrication 2017: Proceedings of the 28th Annual International Solid Freeform Fabrication Symposium; 2017.
[143] http://www.imprintenergy.com.

[144] Wang Y, Diaz DFR, Chen KS, Wang Z, Adroher XC. Materials, technological status, and fundamentals of PEM fuel cells–a review. Mater Today 2019.
[145] https://www.energy.gov/eere/fuelcells/doe-technical-targets-hydrogen-production-electrolysis.
[146] Alkahari MR, Furumoto T, Ueda T, Hosokawa A. Melt pool and single track formation in selective laser sintering/selective laser melting. Adv. Mater. Res. 2014;933:196–201.
[147] Craeghs T, Bechmann F, Berumen S, Kruth J-P. Feedback control of layerwise laser melting using optical sensors. Physics Procedia 2010;5:505–14.
[148] Doubenskaia M, Pavlov M, Chivel Y. Optical system for on-line monitoring and temperature control in selective laser melting technology. In: Key engineering materials; 2010. Trans Tech Publ.
[149] Berumen S, Bechmann F, Lindner S, Kruth J-P, Craeghs T. Quality control of laser-and powder bed-based Additive Manufacturing (AM) technologies. Physics Procedia 2010;5:617–22.
[150] Doubenskaia M, Pavlov M, Grigoriev S, Tikhonova E, Smurov I. Comprehensive optical monitoring of selective laser melting. J Laser Micro/Nanoeng 2012;7(3).
[151] Bartlett JL, Heim FM, Murty YV, Li X. In situ defect detection in selective laser melting via full-field infrared thermography. Addit Manuf 2018;24:595–605.
[152] Clijsters S, Craeghs T, Buls S, Kempen K, Kruth J-P. In situ quality control of the selective laser melting process using a high-speed, real-time melt pool monitoring system. Int J Adv Manufact Technol 2014;75(5–8):1089–101.
[153] Kanko JA, Sibley AP, Fraser JM. In situ morphology-based defect detection of selective laser melting through inline coherent imaging. J Mater Process Technol 2016;231:488–500.
[154] Markl M, Körner C. Multiscale modeling of powder bed–based additive manufacturing. Annu Rev Mater Res 2016;46:93–123.
[155] Wang L, Felicelli S, Gooroochurn Y, Wang P, Horstemeyer M. Optimization of the LENS® process for steady molten pool size. Mater Sci Eng A 2008;474(1–2):148–56.
[156] Tsirkas S, Papanikos P, Kermanidis T. Numerical simulation of the laser welding process in butt-joint specimens. J Mater Process Technol 2003;134(1):59–69.
[157] Shen N, Chou K. Thermal modeling of electron beam additive manufacturing process: powder sintering effects. In: ASME 2012 International Manufacturing Science and Engineering Conference 2012. American Society of Mechanical Engineers Digital Collection.
[158] Hongyuan F, Qingguo M, Wenli X, Shude J. New general double ellipsoid heat source model. Sci Technol Weld Joining 2005;10(3):361–8.
[159] Dunbar AJ, Denlinger ER, Gouge MF, Michaleris P. Experimental validation of finite element modeling for laser powder bed fusion deformation. Addit Manuf 2016;12:108–20.
[160] Unocic R, DuPont J. Process efficiency measurements in the laser engineered net shaping process. Metall Mater Trans B 2004;35(1):143–52.
[161] Klassen A, Scharowsky T, Körner C. Evaporation model for beam based additive manufacturing using free surface lattice Boltzmann methods. J Phys D Appl Phys 2014;47(27):275303.
[162] Lee YS, Zhang W. Modeling of heat transfer, fluid flow and solidification microstructure of nickel-base superalloy fabricated by laser powder bed fusion. Addit Manuf 2016;12:178–88.
[163] Gürtler F-J, Karg M, Leitz K-H, Schmidt M. Simulation of laser beam melting of steel powders using the three-dimensional volume of fluid method. Physics Procedia 2013;41:881–6.
[164] Tapia G, Khairallah S, Matthews M, King WE, Elwany A. Gaussian process-based surrogate modeling framework for process planning in laser powder-bed fusion additive manufacturing of 316L stainless steel. Int J Adv Manufact Technol 2018;94(9–12):3591–603.
[165] Vo TQ, Kim BH. Molecular dynamics study of thermodynamic properties of nanoclusters for additive manufacturing. Int J Precis Eng Manufact-Green Technol 2017;4(3):301–6.
[166] Ji Y, Dong C, Kong D, Li X. Design materials based on simulation results of silicon induced segregation at AlSi10Mg interface fabricated by selective laser melting. J Mater Sci Technol 2020;46:145–55.
[167] Mukherjee T, Wei H, De A, DebRoy T. Heat and fluid flow in additive manufacturing–Part II: Powder bed fusion of stainless steel, and titanium, nickel and aluminum base alloys. Comput Mater Sci 2018;150:369–80.
[168] Khairallah SA, Anderson A. Mesoscopic simulation model of selective laser melting of stainless steel powder. J Mater Process Technol 2014;214(11):2627–36.
[169] Mukherjee T, Manvatkar V, De A, DebRoy T. Dimensionless numbers in additive manufacturing. J Appl Phys 2017;121(6):064904.
[170] Kamath C. Data mining and statistical inference in selective laser melting. Int J Adv Manufact Technol 2016;86(5–8):1659–77.
[171] Niu Z, Wang Y, Jiao K, Wu J. Two-phase flow dynamics in the gas diffusion layer of proton exchange membrane fuel cells: volume of fluid modeling and comparison with experiment. J Electrochem Soc 2018;165(9):F613–20.
[172] Lee Y, Zhang W. Mesoscopic simulation of heat transfer and fluid flow in laser powder bed additive manufacturing. In: International Solid Free Form Fabrication Symposium, Austin; 2015.
[173] Shan X, Chen H. Lattice Boltzmann model for simulating flows with multiple phases and components. Phys Rev E 1993;47(3):1815.
[174] Wang Y, Wei Q, Pan F, Yang M, Wei S. Molecular dynamics simulations for the examination of mechanical properties of hydroxyapatite/poly α-n-butyl cyanoacrylate under additive manufacturing. Bio-Med Mater Eng 2014;24(1):825–33.
[175] Zhou W, Kikuchi K, Nomura N, Yoshimi K, Kawasaki A. In-situ formation of ceramic layer on Mo-based composites via laser powder bed fusion. Materialia 2020;10:100655.
[176] So KP, Kushima A, Park JG, Liu X, Keum DH, Jeong HY, et al. Intragranular dispersion of carbon nanotubes comprehensively improves aluminum alloys. Adv Sci 2018;5(7):1800115.
[177] So KP, Liu X, Mori H, Kushima A, Park JG, Kim HS, et al. Ton-scale metal–carbon nanotube composite: the mechanism of strengthening while retaining tensile ductility. Extreme Mech Lett 2016;8:245–50.
[178] So KP, Chen D, Kushima A, Li M, Kim S, Yang Y, et al. Dispersion of carbon nanotubes in aluminum improves radiation resistance. Nano Energy 2016;22:319–27.